Meiotic prophase length modulates Tel1-dependent DNA double-strand break interference

Luz María López Ruiz[1], Dominic Johnson, William H. Gittens, George Brown, Rachal M. Allison, and Matthew J. Neale[1]

Genome Damage and Stability Centre, School of Life Sciences, University of Sussex, UK

1. For correspondence: m.neale@sussex.ac.uk; L.Lpez-Ruiz@sussex.ac.uk

ABSTRACT

During meiosis, genetic recombination is initiated by the formation of many DNA double-strand breaks (DSBs) catalysed by the evolutionarily conserved topoisomerase-like enzyme, Spo11, in preferred genomic sites known as hotspots. DSB formation activates the Tel1/ATM DNA damage responsive (DDR) kinase, locally inhibiting Spo11 activity in adjacent hotspots via a process known as DSB interference. Intriguingly, in *S. cerevisiae*, over short genomic distances (<15 kb), Spo11 activity displays characteristics of concerted activity or clustering, wherein the frequency of DSB formation in adjacent hotspots is greater than expected by chance. We have proposed that clustering is caused by a limited number of sub-chromosomal domains becoming primed for DSB formation. Here, we demonstrate that DSB clustering is abolished when meiotic prophase timing is extended via deletion of the *NDT80* transcription factor. We propose that extension of meiotic prophase enables most cells, and therefore most chromosomal domains within them, to reach an equilibrium state of similar Spo11-DSB potential, reducing the impact that priming has on estimates of coincident DSB formation. Consistent with this view, genome-wide maps of Spo11-DSB formation generated in the absence of Tel1 are skewed towards regions that load pro-DSB factors early—revealing regions of preferential priming—but this effect is abolished when *NDT80* is deleted. Our work highlights how the stochastic nature of Spo11-DSB formation in individual cells within the limited temporal window of meiotic prophase can cause localised DSB clustering—a phenomenon that is exacerbated in *tel1*Δ cells due to the dual roles that Tel1 has in DSB interference and meiotic prophase checkpoint control.

INTRODUCTION

During meiosis, DNA double-strand breaks (DSBs) created by the evolutionarily conserved topoisomerase-like protein, Spo11, form in a highly regulated manner in order to initiate genetic recombination between homologous chromosomes[1–3]. Pairing of homologous chromosomes, mediated by this recombination process, facilitates homologue alignment during prophase I and subsequent accurate segregation[4,5]. Consequently, failures of either the initiation or completion of recombination can lead to chromosome segregation errors, generating inviable gametes[4,6,7].

The regulation of Spo11 activity arises at multiple levels that affect when, where, and how frequently DSBs are created across the genome[8–11]. In the sexually reproducing budding yeast *Saccharomyces cerevisiae* nine additional proteins are absolutely required for Spo11 activity, many of which have conserved functions in other species[12]. Rec102, Rec104 and Ski8, form the catalytic core with Spo11[13,14], generating a complex with structural similarity to the ancestral heterotetrameric protein Topoisomerase VI[1,14–18]. Rec114, Mer2 and Mei4 interact with one another, bind to the structural axis of the meiotic chromosome, and are thought to regulate core-complex assembly and/or catalysis[19–22]. Finally, the evolutionarily conserved Mre11 complex (Mre11, Rad50 and Xrs2/Nbs1), has roles in both the formation and in the repair of Spo11-DSBs, the latter role performed alongside a critical repair factor component, Sae2, the orthologue of human CtIP[3,23–28]. In the absence of Sae2 (also known as Com1), Spo11-DSBs accumulate with Spo11 remaining covalently bound to DSB ends via a 5′ phospho-tyrosine linkage[29–35]—consistent with Spo11's topoisomerase-like mechanism of DSB formation—enabling locus-specific and genome-wide measurements of Spo11-DSB formation[36–39].

In *S. cerevisiae*, around 150–200 DSBs are generated during the leptotene-zygotene stages of meiotic prophase, and are spread in a nonuniform manner across the four copies (two homologues, each with two sister chromatids) of the 16 chromosomes—a total of ~50 Mbp of genomic DNA[38,40,41]. When assayed in a population of cells, Spo11 DSBs are found to form preferentially in regions of nucleosome depletion and are termed hotspots[38,42,43]. Spo11-DSB frequency within hotspots is influenced by many proactive features of the chromosome topography, including DNA replication dynamics[44–46], gene organisation[38,47], cohesin binding[48,49] and nucleosome modification[38,50,51], alongside higher-order chromosomal architectures such as centromeres, telomeres[38,40,47,52,53] and repetitive elements[38,54,55], which collectively influence the local and broad-range loading of Spo11 and other pro-DSB factors to chromosomes[19,38,47]. In addition, greater-than-expected coincidence of Spo11-DSB formation in adjacent hotspots[56] (clustering), suggests that on a per-cell basis, subdomains of

pro-DSB activity assemble upstream of DSB cleavage at different locations in different cells[10,56], but what defines and regulates their formation is unclear.

Spo11-DSB formation is also regulated reactively. As a potentially toxic DNA lesion, unrepaired Spo11 DSBs are recognised by the DNA damage response (DDR) kinases Tel1 and Mec1, the *S. cerevisiae* orthologues of the human checkpoint kinases Ataxia Telangiectasia Mutated (ATM) and AT-related (ATR), respectively[57]. Tel1 activation directly inhibits further Spo11-DSB formation in a process described as DSB interference[56,58–60]. Such negative regulation appears to act relatively locally, reducing the probability of coincident DSBs arising in adjacent hotspots, a phenomenon otherwise referred to as inter-hotspot double cutting[56]. Notably, such inhibition indirectly reduces the global Spo11-DSB frequency[56,59–61], including a reduction in the formation of hyper-localised double cuts (DCs) that form within Spo11 hotspots[41,62].

Despite clear roles for Tel1 in the negative regulation of Spo11 (a conserved role carried out by ATM in mouse, plants, and flies[63–68]), the critical target(s) of the Tel1 kinase that translate such negative regulation remain obscure, with Rec114 the main lead[59,60,69]. Tel1, and its sister kinase, Mec1, also have roles in biasing DSBs to repair using the homologous chromosome and in checkpoint activation—delaying the onset of meiotic nuclear divisions as part of the DNA damage response—both via activation of the meiosis-specific Rad53/CHK2 orthologue, Mek1[70–76]. Furthermore, global down-regulation of Spo11-DSB formation is mediated via both the establishment of successful homologous chromosome interaction (termed homologue engagement[77]) and by the checkpoint-regulated exit from meiotic prophase via activation of the Ndt80 transcription factor[59], which is involved in the regulation of genes involved in later stages of sporulation[73,78–82]. Thus, whilst some activities of Tel1 promote meiosis-specific modes of DSB repair, contemporaneous checkpoint activation—mediated by Tel1 and others—may increase the time that cells remain in earlier stages of meiotic prophase, and thereby remain in a DSB-permissive state. However, precisely whether and how DSB interference is affected by prophase timing regulation has not been characterised.

Here, we utilise deletion of *NDT80* to explore the influence that meiotic prophase kinetics has on the process of Tel1-dependent DSB interference using both locus-specific assays and by assessing changes to the global genome-wide patterns of Spo11-DSB formation. We demonstrate that short-range DSB interference—and the manifestation of clustering—is modulated by prophase length. We further provide evidence that genome-wide patterns of DSB formation are influenced by both Tel1 and Ndt80—the latter of which we exploit to reveal chromosomal domains of preferred DSB activity.

RESULTS

Deletion of *TEL1* accelerates exit from meiotic prophase in *sae2*Δ cells

We previously demonstrated that Spo11-dependent DNA double-strand break (DSB) formation in *S. cerevisiae* is reactively inhibited in response to a proximal DSB, via the evolutionarily conserved PIKK kinase, Tel1[56] (**Fig 1a**). Importantly, Tel1 has been implicated in prophase checkpoint activation in *rad50S* cells—in which Spo11 DSBs accumulate without resection—causing *TEL1* mutants to exit meiotic prophase prematurely[70]. Similarly, we hypothesised that abrogation of Tel1 activity might also accelerate prophase exit (**Fig S1a**), reducing the time-window of opportunity for DSB formation in the cell populations used for our studies, which employed a deletion of the Mre11 nuclease cofactor, *SAE2*, in order to permit unresected Spo11-DSB signals to accumulate[25,26,29,31].

To test this idea, we compared meiotic prophase kinetics by monitoring the time at which cells completed the first meiotic nuclear division (MI) in synchronised meiotic cultures (**Fig 1b, S1b-d**). Whilst wild-type cultures started to initiate MI at ~5 hours, with MI complete in 80% of the population by 10 hours, *sae2*Δ cells were delayed by ~2-3 hours (**Fig 1b**), similar to *rad50S* mutants[70]. By contrast—but again like in the *rad50S* background[70]—deletion of *TEL1* in the *sae2*Δ background substantially rescued this delay (**Fig 1b**).

These observations confirm that *sae2*Δ cells exit meiotic prophase earlier in the absence of Tel1, which may cause some cells to have less opportunity to initiate Spo11-DSB formation than in the presence of Tel1.

Deletion of *NDT80* increases DSB formation in the absence of Tel1

We hypothesised that deletion of the *NDT80* transcription factor, causing meiotic cells to arrest permanently in late prophase[81], might equalise the length of time cells remain in prophase—and thus their DSB-forming potential—independently of the presence or absence of Tel1 activity (**Fig S1e**). To test this idea, we first determined the impact of extending meiotic prophase (*NDT80* deletion) on the overall frequency of DSB formation at a number of strong hotspots previously used to assess DSB interference[56]: *HIS4*::*LEU2* (**Fig 1c**), *ARE1* (**Fig S2a**), and *YCR061W* (**Fig S3a**).

At *HIS4*::*LEU2*, DSB frequency increased over time reaching a maximum at 6-8 h after meiotic induction of ~10% at site I and ~5% at site II in the *sae2*Δ control (**Fig 1d-g**), frequencies that were not substantially altered upon *NDT80* deletion (**Fig 1f-h**). As previously reported[56], deletion of *TEL1* in the *sae2*Δ background increased DSB frequency by around ~1.5-fold at both sites (**Fig 1d-h**). Remarkably, however, DSB frequency was further elevated (by almost

two-fold) in the *sae2*Δ *tel1*Δ *ndt80*Δ triple mutant, with total (DSB I + DSB II) levels reaching ~46% of total DNA (**Fig 1h**). Notably, DSB I signals, as measured with the *MXR2* probe, showed partial smearing down the gel suggesting a general increase in hotspot width, perhaps caused by the increase in the frequency of hyper-localised coincident cutting by Spo11 that arises within hotspots[41,62] (**Fig 1d**).

DSB frequencies measured around the *ARE1* locus were both increased by deletion of *NDT80* in the *sae2*Δ *tel1*Δ background, reaching levels higher than those previously reported for when Ndt80 is present[56] (**Fig S2b-f**). At the *YCR061W* locus, the effect at individual hotspots varied (**Fig S3b-f**). Hotspot 'N' was increased by *TEL1* deletion, but not further by *NDT80* deletion (**Fig S3d**), whereas hotspot 'Q' was increased more by *NDT80* deletion than by *TEL1* deletion (**Fig S3f**). Notably, deletion of *TEL1* leads to the formation of a previously undetectable hotspot "O" (**Fig S3c**) flanking the *YCR061WI* probe (also detected in genome-wide CC-seq[39] maps of Spo11 DSBs; **Fig S3a**), and this hotspot was increased a further two-fold upon *NDT80* deletion (**Fig S3e**).

Collectively, such observations support the view that early exit from meiotic prophase that happens in *sae2*Δ *tel1*Δ cells leads to an underestimate of the total DSB potential that is possible when Tel1 is absent, and that this can be revealed by arresting cells in late meiotic prophase via *NDT80* deletion.

Deletion of *NDT80* alters measurements of DSB interference over short range

In prior work we determined that, rather than just displaying loss of DSB interference in the absence of Tel1, over short genomic distances Spo11 DSBs were found to arise coincidently more often than expected by chance—a phenomenon referred to as negative interference and/or clustering (**Fig 1a**, inset). We previously hypothesised that this clustering effect arises due to activation of DSB formation within a subset of meiotic chromatin loop domains[56]**.** Such apparent clustering can arise when an assayed population is nonhomogeneous—for example when it contains a population of active and inactive loci and/or cells—which could become especially apparent within the shortened prophase of *tel1*Δ cells.

Thus, to test the idea that differences in prophase length could explain our observation of negative interference and DSB clustering, we sought to re-measure DSB interference in the absence of Ndt80—which we hypothesised would increase the homogeneity of the assayed cell population. DSB interference was measured, as in our prior study (see **Fig S1f-l** for a description of the general method of calculation), at the *HIS4*::*LEU2* locus on chromosome III, in which the pair of strong Spo11 DSBs are separated by just 2.4 kb (**Fig 1c**).

Interference was assessed by comparing the observed frequency of coincident DSBs ('double-cuts'; 'DCs', measured with the *LEU2* probe; **Fig 1i-k**) to the product of the frequency (expected) of each individual DSB (DSB I and DSB II; **Fig 1l**) measured using the *MXR2* and *HIS4* probes on the left and right of the locus respectively (**Fig 1c-h**; see Extended methods, "Calculation of DSB interference" for full description). Because DSBs and DCs accumulated over time (**Fig 1f-g,j**), to simplify analysis and reduce sampling error, the 6 and 8 hour time points were averaged, and then this average value was calculated across a number of independent experimental repeats made in both the *NDT80*+ control (n=6) and *ndt80*Δ mutant (n=5) backgrounds (**Fig 1h,k**).

Aggregation of additional observations made in this study with prior measurements[56] reinforced the prior conclusion: that is, in the presence of Tel1, a similar frequency of DCs were observed to those that were expected (**Fig 1l**), suggesting no interference over this short distance even though Tel1 is present (and thus the formation of DCs inhibited; **Fig 1m**). *TEL1* deletion led to a ~1.5-fold increase in the frequency of single DSBs (**Fig 1h**), but a disproportionate ~10-fold increase in the frequency of DCs (**Fig 1k**)—demonstrating not just Tel1's inhibitory role, but also how observed DCs then exceed by ~3-fold those expected by chance alone (**Fig 1l**), leading to a negative interference calculation (**Fig 1m**).

Remarkably, in the presence of Tel1—but now in the absence of Ndt80—although single DSB frequency increased a small amount (**Fig 1h**), DC frequency was unchanged (**Fig 1k**), and at a lower frequency than expected (**Fig 1l**), leading to positive interference (**Fig 1m**). Moreover, in the absence of Tel1 and Ndt80, single DSB frequencies increased further (**Fig 1h**), but without any increase in DCs relative to *tel1*Δ (**Fig 1k**), leading observed and expected frequencies of DCs to be similar (**Fig 1l**), and therefore, an absence of interference (**Fig 1m**).

To test whether similar effects were observed elsewhere, we also measured DSB and DC formation between the three main hotspots (labelled 'E', 'F', and 'I') flanking the *BUD23–ARE1* locus on chromosome III[56] (**Fig S2a**). Although other minor DSBs (and thus DCs) are also visible, their low cutting frequency and the relatively high lane background precluded their accurate measurement in this study. Deletion of *NDT80* increased single DSB frequencies in both the presence and the absence of Tel1 (**Fig S2b-f**) but without any major changes in DC frequencies relative to the large effect caused by *TEL1* deletion (**Fig S2g-j**). In agreement with the measurements made at *HIS4*::*LEU2* above, these effects altered DSB interference (**Fig S2k-n**) such that control *TEL1*+ *ndt80*Δ cells displayed strong positive interference (**Fig S2m-**

n; rather than weak interference), and *tel1*Δ *ndt80*Δ cells now displayed weak/absent interference (**Fig S2m-n**; rather than strong negative interference).

DSB interference measurements at a third locus (*YCR061W*) were more complicated, although displaying some similar trends (**Fig S3**). Measuring DC formation between the main hotspot, 'N', and hotspot 'Q', 3.7 kb away (**Fig S3g-i**), and therein calculating DSB interference (**Fig S3j-m**), showed that—similar to at *HIS4*::*LEU2* and *ARE1*—deletion of *NDT80* when Tel1 is absent causes a substantial reduction in the negative interference previously observed[56] between hotspots N and Q (**Fig S3l**). However, potentially due to low signals and relatively high background levels (**Fig S3g-h**), we were unable to detect any change in interference upon deletion of *NDT80* in the presence of Tel1 (**Fig S3l**; see Extended Methods for more details). There was also no measured change in (the negative) interference detected between hotspot N and the new hotspot, O, that arises only in the *tel1*Δ background (above, **Fig S3a,m**)—possibly due to a combination of O being a weak, dispersed hotspot, the very short distance between hotspot N and O (~0.7 kb), and the partially overlapping probe location (see Extended Methods for more details).

In summary, whilst somewhat variable at individual loci, these observations support the view that the previously intriguing observation that over short distances Spo11 DSBs failed to display interference in the presence of Tel1 and displayed negative interference in the absence of Tel1, is influenced by Ndt80. Specifically, when meiotic prophase is extended via *NDT80* deletion, adjacent DSBs now generally display positive interference in the presence of Tel1, but little or no interference in the absence of Tel1.

Deletion of *NDT80* does not alter DSB interference over medium distances

We next explored the impact of deleting *NDT80* on DSB interference measured over medium distances (**Fig 2; Fig S4**)—starting with the ~28 kb interval between the *HIS4*::*LEU2* and *leu2*::*hisG* hotspot loci inserted on the left arm of chromosome III[56] (**Fig 2a**). As measured using a probe close to the end of the chromosome (*CHA1*), deletion of *NDT80* and/or deletion of *TEL1* led to an increase in DSB formation at *HIS4*::*LEU2*, and in an additive manner (**Fig 2b-c**). By contrast, DSB measurements at the *leu2*::*hisG* locus were more variable, on average displaying no clear trend (**Fig 2d**).

Whilst DCs between *HIS4*::*LEU2* and *leu2*::*hisG* (measured by the *FRM2* probe) were at or below the detection limit in the presence of Tel1, DCs were readily induced in the absence of Tel1 (**Fig 2e-f**). Deletion of *NDT80* had little effect on DC formation in the presence of Tel1, but caused a substantial (albeit variable) increase in the absence of Tel1 (**Fig 2e-f**).

Importantly, the concomitant increases in both single DSB frequencies (**Fig 2c**) and DC frequencies (**Fig 2f**) upon *NDT80* deletion, generated no changes in the ratios of observed to expected DC formation (**Fig 2g**), and as a result no change in measurements of DSB interference between these loci (**Fig 2h**).

In agreement with these findings, measuring DSB and DC frequencies and DSB interference between the *ARE1* and *YCR061W* loci, separated by ~14 kb (**Fig S4a**), demonstrated that although DC frequencies were modestly increased upon *NDT80* deletion (both in the presence and absence of Tel1; **Fig S4b**), this did not change the measurements of DSB interference (**Fig S4c**).

Taken together, these observations underscore the view that whilst Tel1-dependent DSB interference acts over both short and medium scales, the observation of negative interference over short distances in *tel1*Δ mutants appears uniquely influenced by *NDT80* status.

Deletion of *NDT80* alters the genome-wide DSB distribution in the absence of Tel1

We recently developed covalent-complex sequencing (CC-seq), a high-resolution and genome-wide sequencing method to detect and characterise the covalent Spo11-DSB intermediates that accumulate in meiosis when *SAE2* is deleted[39] (**Fig 3a**). Based on the observations made above, we next sought to use CC-seq to explore the effects that Ndt80 and Tel1 may have on DSB formation at a genome-wide scale.

Taking the lead from prior work that mapped the transient Spo11-oligo intermediates liberated from Spo11-DSB ends in wild-type cells[38,60], we first simplified the data into a set of ~3400 Spo11-DSB hotspots characterised by their local enrichment of reads (**Fig S5a**). The locations of these hotspots overlapped well (>85% congruence) with prior hotspot positions called from Spo11-oligo data in wild-type cells[38,60] (**Fig S5b-c**). Residual differences are likely caused by a combination of methodological (Spo11-oligo seq vs CC-seq) and real (*SAE2*+ vs *sae2*Δ genotypes, and presence/absence of tags on Spo11 itself) effects, and were disproportionately associated with weaker hotspots (**Fig S5d-f**). Notably, only a minority (32/3473; <1%) of hotspots called from the CC-seq data were also present in a *sae2*Δ *ndt80*Δ *spo11-Y135F* control sample in which the catalytic activity of Spo11 is disabled (**Fig S5g**), and these were all weak (**Fig S5h**), underscoring the utility of CC-seq for measuring bona fide Spo11-DSB formation at a genome-wide scale.

Hotspot strengths were highly positively correlated between *sae2*Δ and *sae2*Δ *ndt80*Δ samples (Pearson R=0.98; **Fig 3b**), but slightly less so in the *sae2*Δ *tel1*Δ and *sae2*Δ *tel1*Δ *ndt80*Δ

samples (Pearson R=0.92; **Fig 3c**), suggesting again that the impact that Ndt80 has is more significant in the absence of Tel1. As expected from the highly correlated Pearson values, at broad scale, hotspot-strength distributions were visually almost indistinguishable between the four datasets when plotted along a representative chromosome (chromosome VII; **Fig 3d**). However, plotting a smoothed ratio of hotspot strength revealed spatial patterns influenced by the presence of Ndt80 that were much stronger in the absence of Tel1 (**Fig 3e**; **Fig S6**).

To characterise these effects on each chromosome, ratios of hotspot strengths ±*NDT80* were represented as heatmaps binned at 50 kb scale (**Fig 3f-g**), and plotted centred on the centromere consistent with prior representations[83]. Effects of Ndt80 in the presence of Tel1 were relatively modest and did not display a clear spatial pattern with respect to chromosome features such as telomeres and the centromere (**Fig 3f**). By contrast, in the absence of Tel1, the presence of Ndt80 led to a dramatic enrichment of Spo11-DSB signal in centromere-proximal regions—notably encompassing the entirety of the three shortest chromosomes (I, III, and VI), and the entire region of chromosome XII left of the rDNA array (**Fig 3g**). These observations suggest that *NDT80* deletion in the *tel1*Δ background promotes genome-wide redistribution of Spo11 activity, generating a more uniform pattern—and preventing bulk enrichment of Spo11 activity in these largely centromere-proximal regions.

To understand how this pattern of enrichment might be explained by other features of Spo11-DSB formation, we compared our fold ratios ±*NDT80* in the *tel1*Δ background to the time that Rec114—an essential pro-DSB factor—associates with meiotic chromosomes[83] (**Fig 3h**). Remarkably, regions of Spo11-DSB formation that are enriched in the *sae2*Δ *tel1*Δ strain are similar to regions that load Rec114 early (**Fig 3g-h**). Given that Rec114 is essential for Spo11-DSB formation[3,12,20,21,84,85], we propose that in the shorter prophase experienced by *sae2*Δ *tel1*Δ cells (data above), DSB formation is enhanced in the subset of chromosome domains in which Rec114 first associates. We further propose that it is this effect that drives the negative DSB interference (DSB clustering) that we have measured over short distances[56].

Tel1 activity patterns DSB hotspot strength across the genome

We thus next sought to take advantage of the *NDT80* deletion-induced meiotic prophase arrest to characterise the specific genome-wide effects caused by loss of Tel1-dependent DSB interference (**Fig 4**). Previous analysis of Spo11-oligo patterns in the presence and absence of Tel1 revealed spatially localised correlated changes in DSB hotspot strengths that decayed with distance (adjacent hotspots either went up or down in a correlated manner), with local inhibition also patterned locally by the insertion of strong DSB hotspots[60]. Globally, however, DSB hotspot strengths measured using Spo11-oligo data in the presence and absence of Tel1

are highly correlated (R=0.97; **Fig 4a**), suggesting relatively weak global effects. By contrast, deletion of *TEL1* affected CC-seq (*sae2*Δ background) hotspot strengths more severely (R=0.91 in *NDT80*+; **Fig 4b**), likely driven at least in part by the *tel1*Δ-dependent alterations in prophase length described above. Nevertheless, even in the absence of Ndt80, CC-seq DSB hotspot strengths ±*TEL1* were less similar in the CC-seq *sae2*Δ data (R=0.94 in *ndt80*Δ; **Fig 4c**) than in the published Spo11-oligo data[60].

It is important to note that in all cases, these Pearson correlation values are high, and consistent with this, like with ±*NDT80* comparisons, broad-scale hotspot-strength distributions were almost visually indistinguishable from one another between the paired ±*TEL*1 dataset comparisons when plotting along a representative chromosome (e.g. chromosome IV; **Fig 4d**). However, plotting a smoothed ratio of hotspot strengths revealed a very different picture (**Fig 4e**; **Fig S7a**). Whereas effects on Spo11-oligo hotspot strength ±*TEL1* were relatively weak and evenly distributed (**Fig 4e**, top panel; **Fig S7a**, left column) deletion of *TEL1* in the CC-seq *sae2*Δ and *sae2*Δ *ndt80*Δ strains revealed strong Tel1-dependent spatially patterned chromosome-specific changes that shared many similar features in both the presence and absence of Ndt80 (**Fig 4e**, middle and lower panels; **Fig S7a**, middle and right columns; **Fig S7b**). The most dramatic effects were often observed towards the ends of many chromosomes—where the distribution of DSBs was enhanced in the presence of Tel1, as was the relative proportion of DSBs forming on the entirety of chromosome 12 (**Fig 4f-g**).

We propose that these chromosome-specific effects are the genome-wide signature of Tel1-dependent DSB interference—manifesting as spatially patterned changes in the population-average frequency of Spo11 DSB formation within hotspots (LLR and MJN; manuscript in preparation). Importantly, although such effects are influenced to some degree by prophase timing, they are in fact largely unaltered by changes in the length of meiotic prophase.

DISCUSSION

We previously established in *S. cerevisiae* that Spo11-DSBs are subject to distance-dependent interference via activation of the DNA-damage-responsive kinase, Tel1—part of a negative-regulatory pathway that appears to be conserved in mice, flies and plants[63–68]. Critically, due to its involvement in the DNA damage response, Tel1 has at least two overlapping roles: DSB interference and regulation of meiotic prophase kinetics, but our understanding of how these two roles intersected was unclear and largely unexplored.

To investigate the relationship between these two roles of Tel1, we have measured the frequency of single and coincident Spo11-DSB formation arising at adjacent hotspots in the

presence and absence of both Tel1 and Ndt80, the latter of which is a critical transcription factor required for exit from meiotic prophase[81]. Importantly, deletion of *NDT80* causes cells to arrest in late meiotic prophase irrespective of the strength of checkpoint activation. In order to estimate total Spo11-DSB formation potential, we have utilised strains in which Mre11-dependent nucleolytic processing of Spo11-capped DSB ends is abolished via deletion of the activator, *SAE2*[29,31], permitting total Spo11-DSB levels to accumulate.

When considering total Spo11-DSB levels, both *TEL1* and *NDT80* deletion independently increased Spo11 activity, with the greatest DSB frequency arising when both genes were deleted (**Fig 1f-h; Fig S2d-f; Fig S3d-f**). Similar estimates of global Spo11-DSB formation in the presence and absence of Tel1 or Ndt80, but in the presence of Sae2, revealed increases similar to those reported here[60,77]. However, the epistatic relationship between Tel1 and Ndt80 has not been explored. Our observations suggest that Tel1 and Ndt80 likely independently limit total Spo11-DSB levels due to their separate roles in DSB interference and regulation of prophase exit, as has been discussed[59,60].

Because total DSB signals accumulate, deletion of *SAE2* also permits the analysis of instances where DSBs arise coincidentally on the same DNA molecule: “inter-hotspot double cuts”. Whilst both *TEL1* and *NDT80* deletion appear, on average, to increase total DSB formation (see above), and lead to increases in the coincidence of DSB formation in hotspots that were relatively distant to one another (medium range; 20-50 kb), the same was not the case for hotspots at close range (<15 kb). Instead, short-range suppression of double cutting largely depends only on Tel1, with modest or negligible increases upon *NDT80* deletion (**Fig 1k**; **Fig S2i,j**; **Fig S3h,i**).

Intriguingly, in our prior work, although we clearly demonstrated Tel1-dependent DSB inhibition, over very short inter-hotspot distances interference was not detected in the presence of Tel1[56]. Moreover, when *TEL1* was deleted, coincidence of Spo11-DSB formation in adjacent hotspots was higher-than-expected[56].

We previously proposed that these effects can arise due to localised activation of chromosomal domains—priming them for Spo11-DSB formation in different locations in each cell[56]. For instance, although there are around ~4000 potential Spo11-DSB hotspots spread across the haploid yeast genome (totalling 16000 in the replicated diploid prophase state), only 100-200 DSBs are catalysed in any given cell (2-4 DSBs per Mbp), thus some aspect(s) of Spo11-DSB formation must be rate-limiting. If it is the activation step that limits total DSB potential, then the frequency of active domains must be limiting, meaning therefore that active

domains vary in their chromosomal location across the cell population. These effects will create a heterogeneous mixture of active and inactive subpopulations when considering any given chromosomal region (**Fig 5a**). Critically, such heterogeneity will give rise to lower-than-expected measurements of DSB interference (**Fig 5a**, bottom).

In wild-type cells, the formation of such subdomains is likely to help disperse a limited amount of DSB potential across the genome. However, in *tel1*Δ, the absence of localised negative regulation will permit efficient coincident cutting by Spo11 at all DSB hotspots located within any local region of activation—detected as negative interference[56] (**Fig 5a**, bottom).

A prediction of the subpopulation explanation is that any process that increases the homogeneity of the cell population will reduce any underestimates of interference strength (i.e. reduce skews towards negativity). Remarkably, here we have established that underestimates of interference strength are abolished upon deletion of *NDT80*—suggesting that the subpopulations inferred to arise in *NDT80*+ cells are caused by the limited time window that cells spend within meiotic prophase.

Furthermore, because of the dual role of Tel1 in both DSB interference and checkpoint activation, loss of Tel1 leads to an accelerated exit from meiotic prophase (**Fig 1b**), presumably due to a relatively earlier activation of Ndt80 and subsequent down-regulation of Spo11-DSB formation[59]. Such effects of Tel1 loss are likely to be more significant in the *sae2*Δ background, where DSB-dependent checkpoint activation is dependent on Tel1[70], which is not the case under conditions where Spo11 has been removed from DSB ends and ssDNA resection has initiated[60,70]. Thus, the differential prophase timing that arises ±*TEL1* in the *sae2*Δ background potentially exacerbates the subpopulation effect. Our observations suggest that by extending the length of prophase, *NDT80* deletion can be used to limit effects caused by differential prophase kinetics, homogenizing the DSB potential across the entire genome and cell population (**Fig 5b**). We contend that this is particularly important when deleting *TEL1*, or other factors, that influence the meiotic prophase checkpoint.

A key feature of our observations is that negative interference (and its abolition upon *NDT80* deletion) was only detected over short distances—behaviour that is consistent with zones of activation being of relatively limited size (<15 kb). Although Spo11-DSB formation arises in the context of a maturing loop-axis chromosome structure organised by cohesins[86], and contains chromatin loops that are within this size range in *S. cerevisiae*[87,88], such active domains may simply coincide with, and co-occur alongside loop formation, but not necessarily depend upon their existence (see pro-DSB section below).

We have also explored the changes in genome-wide patterns of Spo11-DSB formation that arise in the presence and absence of Tel1, and how these differences are affected by *NDT80* deletion (**Fig 3**). Importantly—and consistent with our hypothesis that accelerated exit from prophase in *sae2*Δ *tel1*Δ accentuates the impact of subpopulation domains in which Spo11 is active—deletion of *NDT80* led to a much stronger change in the genome-wide pattern of DSB formation in *sae2*Δ *tel1*Δ cells than in *sae2*Δ cells (**Fig 3f-g**). Such a difference is expected due to the more limited temporal window of meiotic prophase that otherwise arises in the absence of Tel1.

Critically, regions where Spo11-DSB activity is greatest in the presence of Ndt80 visually correlate with regions that load Rec114 and Mer2 early in meiosis[83] (**Fig 3g-h**), arguing that when the temporal window of meiotic prophase is limited, DSBs tend to arise more often in those regions that load pro-DSB components more efficiently. By contrast, when the duration of meiotic prophase is extended (by *NDT80* deletion), DSBs now arise more evenly across the genome—with a disproportionate enhancement in regions that load pro-DSB factors late.

In general terms, we propose that it is the disproportionate loading of pro-DSB factors in some genomic regions that drives the negative DSB interference (DSB clustering) detected over short distances upon *TEL1* deletion[56]. Precisely how Rec114, Mer2 and Mei4 regulate Spo11-DSB formation remains to be elucidated, however, their potential to form limited amounts[20,21,89] of intermolecular condensates[22], which may generate a surface for Spo11-DSB formation[22,41], makes them prime candidates for generating chromosome-associated domains of local Spo11-DSB potential.

A second finding that emerges from our genome-wide studies, is that despite the influence that temporal changes in meiotic prophase timing has on Spo11-DSB distribution, deletion of *TEL1* itself elicits a much stronger effect that is detectable both in the presence and absence of Ndt80 (**Fig 4f-g**). We hypothesise that these strong Tel1-dependent changes are the genome-wide consequence of DSB interference (LLR & MJN, in preparation), and are robust to changes in the length of meiotic prophase.

A feature—but also a limitation—of our analytical methods is the reliance on *SAE2* deletion to permit Spo11-DSB and Spo11 double-cut signals to accumulate without repair. On the one hand, *sae2*Δ enables us to study mechanisms of DSB interference in the absence of other regulatory pathways that are dependent upon and triggered after Spo11 removal (i.e. homologue engagement[77,90]), and which may otherwise obscure Tel1's influence. However,

we cannot exclude that the accumulation of unrepaired Spo11 DSBs itself influences how the system behaves, and as such, all observations must be interpreted with this in mind.

Looking more broadly, the regulatory feedback mechanisms discussed here are likely to ensure that cells stay in a DSB-permissive state only for as long as needed—limiting the level of DSB formation, and therefore recombination, required to facilitate accurate chromosome pairing and, by extension, efficient chromosome segregation without risk of aneuploidy. Because of Ndt80's role as a transcription factor we favour that the effect Ndt80 elicits is global, influencing the length of time any individual cell remains in meiotic prophase. However, it is also possible that targets of Ndt80 act locally to suppress and inhibit Spo11 activity, directly creating heterogeneity in which chromosomal regions are active within individual cells. Regardless of mechanism, our observations highlight how restrictions on global Spo11 activity can generate subdomains of concerted activity—influencing both localised and population-average patterns of genetic recombination.

AUTHOR CONTRIBUTIONS

LLR and MJN devised the study, analysed and interpreted the observations, and wrote the paper. LLR prepared the figures and performed the experiments with additional contributions from DJ, GB and RMA. WHG and GB contributed to the development of analytical tools.

ACKNOWLEDGEMENTS

We thank S. Keeney, J. Carballo and M. Lichten for sharing *S. cerevisiae* strains containing relevant constructs *(spo11-Y135F*::*KanMX*, *tel1*Δ::hphNT2 and *sae2*Δ::kanMX6, respectively), and K. Caldecott and A. Oliver for sharing recombinant TDP2. LLR, MJN, DJ, WHG, GB, RMA were supported by an ERC Consolidator Grant (311336), the BBSRC (BB/M010279/1), the Wellcome Trust (200843/Z/16/Z), and a Career Development Award from the Human Frontier Science Program (CDA00060/2010). WHG is currently supported by a BBSRC Discovery Fellowship (BB/V005081/1).

DATA ACCESSIBILITY

Raw libraries are available from the GEO repository under accession number (pending). Processed hotspot average table files and analysis scripts are available at **https://github.com/Neale-Lab/Ndt80_LLR**.

MATERIAL AND METHODS

Yeast strains

All the *Saccharomyces cerevisiae* yeast strains used in this study are in the SK1 background as described in **Table S1**, and derived using standard techniques. Strains contained the *his4X*::*LEU2* and *leu2*::*hisG* exogenous sequences inserted on chromosome III[39,41], and carried the *ndt80Δ::LEU2, tel1Δ*::*HphMX4* and/or *sae2Δ*::*kanMX* gene disruption alleles[56,74,81,91]. The *spo11-Y135F*::*KanMX* allele contains an inactivating mutation of the catalytic tyrosine residue[16].

Culture methods

For meiosis induction, a single colony was inoculated in 4mL of YPD medium (1% yeast extract, 2% peptone, 2% glucose supplemented with 0.5 mM adenine and 0.4 mM uracil) and incubated at 30 °C, 250 rpm for a day to reach saturation, then diluted to OD600 of 0.2 in a volume of 200 mL of either YPA (1% yeast extract, 2% peptone, 1% potassium acetate) or SPS (0.5% yeast extract, 1% peptone, 0.67% Yeast Nitrogen Base without amino acids, 1% potassium acetate, 0.05M Potassium Hydrogen phthalate, 0.001% Antifoam 204) pre-sporulation medium. Cultures were incubated at 30 °C, 250 rpm for 14–16 hours, then washed and resuspended in 200 mL pre-warmed SPM sporulation medium (2% potassium acetate supplemented with diluted amino acids) and incubated at 30°C, 250rpm for the duration of the time course. Samples were taken at the relevant timepoints and processed differently. For DNA extraction, 20 mL of culture was taken at t = 0, 4, 6 and 8 hours after inducing meiosis. Samples were centrifuged at 3000 x *g* for 4 minutes, supernatant was discarded and pellet resuspended in 2 mL 50 mM EDTA, centrifuged again for 1 minute at 3000 x *g*, supernatant discarded and pellet stored at -20 °C until use. For Spo11 CC-seq, 50 mL of culture was taken at t = 6 hours. Samples were centrifuged at 3000 x *g* for 5 minutes, supernatant discarded and pellet frozen at -20 °C until use. For FACS, 200 uL of culture was taken at t = 0, 2, 4, 6 and 8 hours after inducing meiosis, samples were centrifuged at 16,000 x *g* for 1 minute, supernatant discarded, fixed in 1mL of 70% EtOH and stored at 4 °C until use. For DAPI staining, 195 uL of culture was taken at t = 3, 4, 5, 5.5, 6, 7, 8, 9 and 10 hours after inducing meiosis. Cells were fixed in 450 uL of 100% EtOH and stored at -20 °C until use.

FACS

Samples were centrifuged at room temperature, 16,000 x *g* for 1 minute. Supernatant was aspirated, pellet resuspended in 500 uL 10 mM Tris HCl pH 8.0 / 15 mM NaCl / 10 mM EDTA pH 8.0 / 1 mg/mL RNase A and incubated at 37°C for 2 hours at 800 rpm on a Eppendorf Thermomixer. Samples were then centrifuged at 16,000 x *g* for 1 minute, supernatant aspirated, pellets resuspended in 100 uL of 1 mg/mL Proteinase K + 50 mM Tris HCl pH 8.0

and incubated at 50°C for 30 minutes at 800 rpm on a Eppendorf Thermomixer. Samples were centrifuged and supernatant aspirated. Pellets were washed in 1 mL 1M Tris-HCl pH 8.0 and then resuspended in 1 mL 50 mM Tris-HCl pH 8.0 + 1 uM Sytox green. Samples were stored overnight at 4 °C and then sonicated at 20% amplitude for 12–14 seconds before being sorted by flow cytometry (Accuri™ Flow Cytometers).

Cell fixation and DAPI staining

Ethanol-fixed cells (4 µL) were dried at RT on a glass slide, stained with 2 µL of Fluoroshield ™ DAPI Sigma-Aldrich (F6057-20ML) and 100–200 mono-, bi-, tri-, tetra-nucleate cells were scored by microscopy (Zeiss AXIO) using fluorescence (CoolLED pE-300 lite). Meiotic progression was determined based on the frequency of cells that entered MI (binucleated) or MII (tri-, tetra-nucleate) at different timepoints after inducing meiosis.

Proteolytic gDNA extraction

Meiotic cell culture pellets were defrosted at room temperature, resuspended in 500 uL of spheroplasting mix: 492.5 uL of spheroplasting buffer (1 M sorbitol / 100 mM NaHPO4 pH 7.2 / 100 mM EDTA), 2.5 uL of zymolyase 100T (50 mg/mL) and 5 uL of β-mercaptoethanol, and incubated at 37 °C for 1 hour. Cells were lysed by adding 100 uL of 3% SDS / 0.1 M EDTA plus 5 uL of Proteinase K (50 mg/mL), and incubated overnight at 60 °C. After cooling to room temperature, proteins were removed with 500 uL of phenol/chloroform: two rounds of vigorous shaking separated by a 5-minute rest and followed by a 5 minutes centrifugation at 14,000 rpm. DNA and RNA were extracted from 450 uL of the aqueous phase and precipitated with 45 uL of 3 M NaAc pH 5.2 and 500 uL of 100% EtOH, centrifuged at 14,000 rpm for 1 minute, aspirated and washed with 1 mL 70% EtOH, pulsed down, air dried for 10 minutes and resuspended in 450 uL of 1x TE (10 mM Tris / 1 mM EDTA pH 7.5) overnight at 4 °C. RNA was digested with 50 uL of 1 mg/mL RNase A (10 mg/ml stock) for 1 hour at 37 °C. DNA was precipitated by addition of 50 uL of NaAc pH 5.2 and 1 mL of 100% EtOH, mixed by inversion and centrifuged for 1 min at 14,000 rpm. DNA was washed with 1 mL 70% EtOH, pulsed down, air dried for 10 minutes, dissolved in 200 uL of 1x TE (10 mM Tris / 1 mM EDTA pH 7.5 prep room solution) overnight at 4 °C. To measure the frequency of DSBs (single-cuts) gDNA was digested with a restriction enzyme (as described in **Table S2**, digestion column). For 20 uL of gDNA, 6 uL of H2O, 3 uL of enzyme buffer and 1 uL of enzyme was added and incubated overnight at 37 °C. To quantify double DSB events (double-cuts), gDNA was left undigested (**Table S2**).

DSB analysis by Southern blot

0.7% or 0.8% agarose gels were prepared for digested and undigested gDNA samples, respectively. The gel was mixed with 125 uL EtBr (0.1 mg/mL) and allowed to set for 1 hour at room temperature. 20 uL of digested sample + 1x loading dye or 10 uL of gDNA + 10 uL water and 1x loading dye was loaded on wells. For the ladder, 10 uL of Lambda BstE II-digest was used as ladder. DNA was separated at 45–50 V for 15–19 hours. Gels were imaged using the Syngene InGenius bioimaging system. DNA was nicked by exposure to 1800 J/m2 UV in a Stratalinker. Afterwards, the gel was soaked in denaturing solution (0.5 M NaOH, 1.5 M NaCl), on a shaker for ~30 minutes.

DSB analysis by PFGE

DNA was embedded in agarose plugs as described below. Agarose plug preparation: Cell pellets were defrosted at room temperature and washed twice with 50 mM cold EDTA (resuspended, spun 1 minute at 4 °C 3000 x g and aspirated). Cells were then resuspended with 135 uL of solution 1 (50 mM EDTA + SCE [Filtered 1 M sorbitol, 0.1 M sodium citrate, 0.06 M EDTA pH 7] + 2% BME + 1 mg/mL zymolyase 100T) and 165 uL of pre-warmed 1% LMP agarose (1% agarose in 0.125M EDTA) at 55 °C. The mix was cooled down at 4 °C for 30 minutes. The solidified plugs were added onto 1 mL of solution 2 (0.45 M EDTA + 20 mM Tris-HCl pH 8 + 1% BME + RNase 10 ug/mL + water) and incubated for 2 hours at 37 °C. Samples were inverted every 30 minutes. Solution 2 was aspirated, and plugs were covered with 1 mL of solution 3 (0.25 M EDTA + 20 mM Tris-HCl pH 8 + 1% sodium sarcosine + 1 mg/mL proteinase K + water) and incubated overnight at 55 °C. Solution 3 was aspirated and samples washed three times with 1 mL of 50 mM EDTA on a rotary wheel. EDTA was aspirated and plugs were covered by 1 mL of storage buffer (50 mM EDTA, 50% glycerol) and stored at -20°C until use. PFGE gel: 1.3% agarose gel was prepared using 150 mL of 0.5X TBE (diluted from 5X TBE: 450 mM tris base + 450 mM boric acid + 10 mM EDTA pH8 + water) and cooled down to 55 °C before use. The plugs were cut in half and washed in 2.5 mL of 0.5X TBE on the rotary wheel for 15 minutes. The plugs were loaded in order onto the gel comb and fixed with 1% agarose. A slice of mid-range PFG marker (#3425, NEB) was fixed onto the first and last gel combs. Once set (10 min at room temperature), the 1.3% agarose was poured covering the gel combs and allowed to solidify for 30 minutes. The gel comb was removed, and wells filled with 1% agarose and allowed to set (10 min at room temperature), then immersed into pre-cooled 0.5X TBE buffer for 15 minutes. For DNA fragments of ~150 kb, the gel was run 30–30s for 3 hours + 3–6s for 37 hours at 6 V/cm and 120 °C angle. After electrophoresis, the gel was soaked in 150 mL distilled water + 7.5 uL of EtBr (0.1 mg/mL), shaken for 20 minutes and then imaged using the Syngene InGenius bioimaging system. DNA

was nicked by exposure to 1800 J/m2 UV in a Stratalinker, then soaked in a denaturing solution (0.5 M NaOH, 1.5 M NaCl) whilst shaking for ~30 minutes.

Southern blotting transfer and hybridisation

The denatured gels were transferred to a Biorad Zeta-probe membrane under vacuum (50–55 mBar for ~2 hours) in 0.5 M NaOH, 1.5 M NaCl. The membrane was washed twice with 2x SSC (diluted from 20x: 3M Sodium chloride, 0.3 M trisodium citrate pH 7.0) and then thrice with distilled water. The membrane was cross-linked by exposure to 1200 J/m2 UV in a Stratalinker, dried at room temperature for 1 hour and stored at 4 °C until probed. Southern Blot membranes were incubated with 35 mL of a pre-warmed hybridisation solution (0.5 M $NaHPO_4$ pH 7.5, 5% SDS, 1 mM EDTA, 1% BSA) at 65 °C for ~1–2 hours. To quantify the single and double DSBs, the membranes were hybridised with an appropriate DNA probe—as indicated in figure legends and **Table S2**—radiolabelled with P_{32} prepared via random priming using the High Prime kit (BioRad). Pre-hybridisation solution was discarded, and the membrane incubated with 20 mL of hybridisation solution containing the radioactive probe overnight at 65 °C. After incubation, the membrane was washed (10% SDS / 1M $NaHPO_4$ / 0.5 M EDTA), air dried, and exposed to a phosphor screen overnight. After exposure (usually 8–48 hours), the phosphoscreen was scanned with a Fuji FLA 5000 reader and analysed using ImageGauge software (Fuji). DSB and DC quantification methods, and limitations of the technique are described in **Extended Methods**.

Covalent complex sequencing (CC-seq) mapping

Protein-DNA Covalent-Complex Mapping (CC-seq) in yeast followed a method previously described[37]. Briefly, meiotic cell samples are chilled and frozen at -20˚C for at least 8 hours, then thawed and spheroplasted (in 1 M sorbitol, 50 mM NaHPO4, 10 mM EDTA, 30 min at 37˚C), fixed in 70% ice-cold ethanol, collected by centrifugation, dried briefly, then lysed in STE (2% SDS, 0.5 M Tris, 10 mM EDTA). Genomic DNA was extracted via Phenol/Chloroform/IAA extraction (25:24:1 ratio) at room temperature, with aqueous material carefully collected, precipitated with ethanol, washed, dried, then resuspended in 1xTE buffer (10 mM Tris/1 mM EDTA). Total genomic DNA was sonicated to <500 bp average length using a Covaris M220 before equilibrating to a final concentration of 0.3 M NaCl, 0.1% TritonX100, 0.05% Sarkosyl. Covalent complexes were enriched on silica columns (Qiagen) via centrifugation, washed with TEN solution (10 mM Tris / 1 mM EDTA / 0.3 M NaCl), before eluted with TES buffer (10 mM Tris / 1 mM EDTA / 1% SDS). Samples were treated with Proteinase K at 50˚C, and purified by ethanol precipitation. DNA ends were filled and repaired using NEB Ultra II end-repair module (NEB #E7645), with adapters ligated sequentially to the sonicated, then blocked, ends with recombinant TDP2 treatment in between these steps to

remove the 5-phosphotyrosyl-linked Spo11 peptide. Ampure bead cleanups were used to facilitate sequential reactions. PCR-amplified libraries were quantified on a Bioanalyser and appropriately diluted and multiplexed for deep sequencing (Illumina MiSeq 2x75 bp).

FASTQ reads were aligned to the reference genome (SacCer3H4L2; which includes the *HIS4*::*LEU2* and *leu2*::*hisG* loci inserted into the Cer3 *S. cerevisiae* genome build[39,41]) via Bowtie2, using TermMapper as previously described[39,41] **(https://github.com/Neale-Lab/terminalMapper)**, with all subsequent analyses performed in R version 4.1.2 using RStudio (Version 2021.09.0 Build 351). Reproducibility between libraries for independent biological replicates was evaluated and validated prior to averaging. For detailed information see **Supplementary scripts**. Details of individual libraries are presented in **Table S3**.

Calibration of CC-seq libraries

For each library the proportion of non-specific reads (background reads) were estimated by measuring the hit rate per million reads per base pair (HpM) in 47 of the longest gene ORFs (> 5.5 kb long) in the *S. cerevisiae* genome. For detailed information about the mechanics of the script, see Calculating background reads.R in **https://github.com/Neale-Lab/Ndt80_LLR**.

Bioinformatic analysis of Spo11-DSB

All bioinformatics analyses were performed in R (R version 4.1.2) using RStudio (Version 2021.09.0 Build 351). Scripts are available on **https://github.com/Neale-Lab/Ndt80_LLR**. For further information see **Script summary description.**

REFERENCES

1. Bergerat, A. et al. An atypical topoisomerase II from Archaea with implications for meiotic recombination. *Nature* **386**, 414-417 (1997).
2. Keeney, S., Giroux, C. N. & Kleckner, N. Meiosis-specific DNA double-strand breaks are catalyzed by Spo11, a member of a widely conserved protein family. *Cell* **88**, 375-384 (1997).
3. Keeney, S. Spo11 and the Formation of DNA Double-Strand Breaks in Meiosis. *Genome dynamics and stability* **2**, 81 (2008).
4. Hunter, N. Meiotic Recombination: The Essence of Heredity. *Cold Spring Harb Perspect Biol* **7**, (2015).
5. Zickler, D. & Kleckner, N. Recombination, Pairing, and Synapsis of Homologs during Meiosis. *Cold Spring Harb Perspect Biol* **7**, (2015).
6. Page, S. L. & Hawley, R. S. Chromosome choreography: the meiotic ballet. *Science* **301**, 785-789 (2003).
7. Petronczki, M., Siomos, M. F. & Nasmyth, K. Un menage a quatre: the molecular biology of chromosome segregation in meiosis. *Cell* **112**, 423-440 (2003).
8. Cooper, T. J., Wardell, K., Garcia, V. & Neale, M. J. Homeostatic regulation of meiotic DSB formation by ATM/ATR. *Exp Cell Res* **329**, 124-131 (2014).
9. Keeney, S., Lange, J. & Mohibullah, N. Self-organization of meiotic recombination initiation: general principles and molecular pathways. *Annu Rev Genet* **48**, 187-214 (2014).

10. Cooper, T. J., Garcia, V. & Neale, M. J. Meiotic DSB patterning: A multifaceted process. *Cell Cycle* **15**, 13-21 (2016).
11. Yadav, V. K. & Claeys Bouuaert, C. Mechanism and Control of Meiotic DNA Double-Strand Break Formation in S. cerevisiae. *Front Cell Dev Biol* **9**, 642737 (2021).
12. Keeney, S. Mechanism and control of meiotic recombination initiation. *Curr Top Dev Biol* **52**, 1-53 (2001).
13. Arora, C., Kee, K., Maleki, S. & Keeney, S. Antiviral protein Ski8 is a direct partner of Spo11 in meiotic DNA break formation, independent of its cytoplasmic role in RNA metabolism. *Mol Cell* **13**, 549-559 (2004).
14. Claeys Bouuaert, C. et al. Structural and functional characterization of the Spo11 core complex. *Nat Struct Mol Biol* **28**, 92-102 (2021).
15. Nichols, M. D., DeAngelis, K., Keck, J. L. & Berger, J. M. Structure and function of an archaeal topoisomerase VI subunit with homology to the meiotic recombination factor Spo11. *EMBO J* **18**, 6177-6188 (1999).
16. Diaz, R. L., Alcid, A. D., Berger, J. M. & Keeney, S. Identification of residues in yeast Spo11p critical for meiotic DNA double-strand break formation. *Mol Cell Biol* **22**, 1106-1115 (2002).
17. Vrielynck, N. et al. A DNA topoisomerase VI-like complex initiates meiotic recombination. *Science* **351**, 939-943 (2016).
18. Robert, T. et al. The TopoVIB-Like protein family is required for meiotic DNA double-strand break formation. *Science* **351**, 943-949 (2016).
19. Panizza, S. et al. Spo11-accessory proteins link double-strand break sites to the chromosome axis in early meiotic recombination. *Cell* **146**, 372-383 (2011).
20. Li, J., Hooker, G. W. & Roeder, G. S. Saccharomyces cerevisiae Mer2, Mei4 and Rec114 form a complex required for meiotic double-strand break formation. *Genetics* **173**, 1969-1981 (2006).
21. Maleki, S., Neale, M. J., Arora, C., Henderson, K. A. & Keeney, S. Interactions between Mei4, Rec114, and other proteins required for meiotic DNA double-strand break formation in Saccharomyces cerevisiae. *Chromosoma* **116**, 471-486 (2007).
22. Claeys Bouuaert, C. et al. DNA-driven condensation assembles the meiotic DNA break machinery. *Nature* **592**, 144-149 (2021).
23. Stracker, T. H. & Petrini, J. H. J. The MRE11 complex: starting from the ends. *Nat Rev Mol Cell Biol* **12**, 90-103 (2011).
24. Neale, M. J., Pan, J. & Keeney, S. Endonucleolytic processing of covalent protein-linked DNA double-strand breaks. *Nature* **436**, 1053-1057 (2005).
25. Cannavo, E. & Cejka, P. Sae2 promotes dsDNA endonuclease activity within Mre11-Rad50-Xrs2 to resect DNA breaks. *Nature* **514**, 122-125 (2014).
26. Cannavo, E. et al. Regulatory control of DNA end resection by Sae2 phosphorylation. *Nat Commun* **9**, 4016 (2018).
27. Cartagena-Lirola, H., Guerini, I., Viscardi, V., Lucchini, G. & Longhese, M. P. Budding Yeast Sae2 is an In Vivo Target of the Mec1 and Tel1 Checkpoint Kinases During Meiosis. *Cell Cycle* **5**, 1549-1559 (2006).
28. Milman, N., Higuchi, E. & Smith, G. R. Meiotic DNA double-strand break repair requires two nucleases, MRN and Ctp1, to produce a single size class of Rec12 (Spo11)-oligonucleotide complexes. *Mol Cell Biol* **29**, 5998-6005 (2009).
29. Keeney, S. & Kleckner, N. Covalent protein-DNA complexes at the 5' strand termini of meiosis-specific double-strand breaks in yeast. *Proc Natl Acad Sci U S A* **92**, 11274-11278 (1995).
30. Prinz, S., Amon, A. & Klein, F. Isolation of COM1, a new gene required to complete meiotic double-strand break-induced recombination in Saccharomyces cerevisiae. *Genetics* **146**, 781-795 (1997).
31. McKee, A. H. & Kleckner, N. A general method for identifying recessive diploid-specific mutations in Saccharomyces cerevisiae, its application to the isolation of mutants blocked at intermediate stages of meiotic prophase and characterization of a new gene SAE2. *Genetics* **146**, 797-816 (1997).
32. Penkner, A. et al. A conserved function for a Caenorhabditis elegans Com1/Sae2/CtIP protein homolog in meiotic recombination. *EMBO J* **26**, 5071-5082 (2007).
33. Uanschou, C. et al. A novel plant gene essential for meiosis is related to the human CtIP and the yeast COM1/SAE2 gene. *EMBO J* **26**, 5061-5070 (2007).
34. Lukaszewicz, A., Howard-Till, R. A., Novatchkova, M., Mochizuki, K. & Loidl, J. MRE11 and COM1/SAE2 are required for double-strand break repair and efficient chromosome pairing during meiosis of the protist Tetrahymena. *Chromosoma* **119**, 505-518 (2010).

35. Hartsuiker, E. et al. Ctp1CtIP and Rad32Mre11 nuclease activity are required for Rec12Spo11 removal, but Rec12Spo11 removal is dispensable for other MRN-dependent meiotic functions. *Mol Cell Biol* **29**, 1671-1681 (2009).
36. Gerton, J. L. et al. Inaugural article: global mapping of meiotic recombination hotspots and coldspots in the yeast Saccharomyces cerevisiae. *Proc Natl Acad Sci U S A* **97**, 11383-11390 (2000).
37. Prieler, S., Penkner, A., Borde, V. & Klein, F. The control of Spo11's interaction with meiotic recombination hotspots. *Genes Dev* **19**, 255-269 (2005).
38. Pan, J. et al. A Hierarchical Combination of Factors Shapes the Genome-wide Topography of Yeast Meiotic Recombination Initiation. *Cell* **144**, 719-731 (2011).
39. Gittens, W. H. et al. A nucleotide resolution map of Top2-linked DNA breaks in the yeast and human genome. *Nature Communications* **10**, (2019).
40. Buhler, C., Borde, V. & Lichten, M. Mapping meiotic single-strand DNA reveals a new landscape of DNA double-strand breaks in *Saccharomyces cerevisiae*. *PLoS Biol* **5**, e324 (2007).
41. Johnson, D. et al. Concerted cutting by Spo11 illuminates meiotic DNA break mechanics. *Nature* **594**, 572-576 (2021).
42. Ohta, K., Shibata, T. & Nicolas, A. Changes in chromatin structure at recombination initiation sites during yeast meiosis. *EMBO J* **13**, 5754-5763 (1994).
43. Wu, T. C. & Lichten, M. Meiosis-induced double-strand break sites determined by yeast chromatin structure. *Science* **263**, 515-518 (1994).
44. Borde, V., Goldman, A. S. & Lichten, M. Direct coupling between meiotic DNA replication and recombination initiation. *Science* **290**, 806-809 (2000).
45. Murakami, H. & Keeney, S. Temporospatial Coordination of Meiotic DNA Replication and Recombination via DDK Recruitment to Replisomes. *Cell* **158**, 861-873 (2014).
46. Blitzblau, H. G., Chan, C. S., Hochwagen, A. & Bell, S. P. Separation of DNA replication from the assembly of break-competent meiotic chromosomes. *PLoS Genet* **8**, e1002643 (2012).
47. Sun, X. et al. Transcription dynamically patterns the meiotic chromosome-axis interface. *Elife* **4**, (2015).
48. Ito, M. et al. Meiotic recombination cold spots in chromosomal cohesion sites. *Genes Cells* **19**, 359-373 (2014).
49. Kugou, K. et al. Rec8 guides canonical Spo11 distribution along yeast meiotic chromosomes. *Mol Biol Cell* **20**, 3064-3076 (2009).
50. Borde, V. et al. Histone H3 lysine 4 trimethylation marks meiotic recombination initiation sites. *EMBO J* **28**, 99-111 (2009).
51. Tischfield, S. E. & Keeney, S. Scale matters: The spatial correlation of yeast meiotic DNA breaks with histone H3 trimethylation is driven largely by independent colocalization at promoters. *Cell Cycle* **11**, (2012).
52. Blitzblau, H. G., Bell, G. W., Rodriguez, J., Bell, S. P. & Hochwagen, A. Mapping of meiotic single-stranded DNA reveals double-stranded-break hotspots near centromeres and telomeres. *Curr Biol* **17**, 2003-2012 (2007).
53. Subramanian, V. V. et al. Persistent DNA-break potential near telomeres increases initiation of meiotic recombination on short chromosomes. *Nat Commun* **10**, 970 (2019).
54. Vader, G. et al. Protection of repetitive DNA borders from self-induced meiotic instability. *Nature* (2011).
55. Sasaki, M., Tischfield, S. E., van Overbeek, M. & Keeney, S. Meiotic Recombination Initiation in and around Retrotransposable Elements in Saccharomyces cerevisiae. *PLoS Genet* **9**, e1003732 (2013).
56. Garcia, V., Gray, S., Allison, R. M., Cooper, T. J. & Neale, M. J. Tel1(ATM)-mediated interference suppresses clustered meiotic double-strand-break formation. *Nature* **520**, 114-118 (2015).
57. Ciccia, A. & Elledge, S. J. The DNA damage response: making it safe to play with knives. *Mol Cell* **40**, 179-204 (2010).
58. Zhang, L., Kleckner, N. E., Storlazzi, A. & Kim, K. P. Meiotic double-strand breaks occur once per pair of (sister) chromatids and, via Mec1/ATR and Tel1/ATM, once per quartet of chromatids. *Proc Natl Acad Sci U S A* **108**, 20036-20041 (2011).
59. Carballo, J. A. et al. Budding Yeast ATM/ATR Control Meiotic Double-Strand Break (DSB) Levels by Down-Regulating Rec114, an Essential Component of the DSB-machinery. *PLoS Genet* **9**, e1003545 (2013).

60. Mohibullah, N. & Keeney, S. Numerical and spatial patterning of yeast meiotic DNA breaks by Tel1. *Genome Res* **27**, 278-288 (2017).
61. Lukaszewicz, A., Lange, J., Keeney, S. & Jasin, M. Control of meiotic double-strand-break formation by ATM: local and global views. *Cell Cycle* **17**, 1155-1172 (2018).
62. Prieler, S. et al. Spo11 generates gaps through concerted cuts at sites of topological stress. *Nature* **594**, 577-582 (2021).
63. Fowler, K. R., Hyppa, R. W., Cromie, G. A. & Smith, G. R. Physical basis for long-distance communication along meiotic chromosomes. *Proceedings of the National Academy of Sciences* 201801920 (2018).
64. Joyce, E. F. et al. Drosophila ATM and ATR have distinct activities in the regulation of meiotic DNA damage and repair. *J Cell Biol* **195**, 359-367 (2011).
65. Lange, J. et al. ATM controls meiotic double-strand-break formation. *Nature* **479**, 237-240 (2011).
66. Lange, J. et al. The Landscape of Mouse Meiotic Double-Strand Break Formation, Processing, and Repair. *Cell* (2016).
67. Lukaszewicz, A., Lange, J., Keeney, S. & Jasin, M. De novo deletions and duplications at recombination hotspots in mouse germlines. *Cell* **184**, 5970-5984.e18 (2021).
68. Kurzbauer, M. T. et al. ATM controls meiotic DNA double-strand break formation and recombination and affects synaptonemal complex organization in plants. *Plant Cell* **33**, 1633-1656 (2021).
69. Guo, H. et al. Phosphoregulation of DSB-1 mediates control of meiotic double-strand break activity. *Elife* **11**, (2022).
70. Usui, T., Ogawa, H. & Petrini, J. H. A DNA damage response pathway controlled by Tel1 and the Mre11 complex. *Mol Cell* **7**, 1255-1266 (2001).
71. Niu, H. et al. Partner choice during meiosis is regulated by Hop1-promoted dimerization of Mek1. *Mol Biol Cell* **16**, 5804-5818 (2005).
72. de los Santos, T. & Hollingsworth, N. M. Red1p, a MEK1-dependent phosphoprotein that physically interacts with Hop1p during meiosis in yeast. *J Biol Chem* **274**, 1783-1790 (1999).
73. Prugar, E., Burnett, C., Chen, X. & Hollingsworth, N. M. Coordination of Double Strand Break Repair and Meiotic Progression in Yeast by a Mek1-Ndt80 Negative Feedback Loop. *Genetics* **206**, 497-512 (2017).
74. Carballo, J. A., Johnson, A. L., Sedgwick, S. G. & Cha, R. S. Phosphorylation of the axial element protein Hop1 by Mec1/Tel1 ensures meiotic interhomolog recombination. *Cell* **132**, 758-770 (2008).
75. Harper, J. W. & Elledge, S. J. The DNA damage response: ten years after. *Mol Cell* **28**, 739-745 (2007).
76. Schwacha, A. & Kleckner, N. Interhomolog bias during meiotic recombination: meiotic functions promote a highly differentiated interhomolog-only pathway. *Cell* **90**, 1123-1135 (1997).
77. Thacker, D., Mohibullah, N., Zhu, X. & Keeney, S. Homologue engagement controls meiotic DNA break number and distribution. *Nature* **510**, 241-246 (2014).
78. Chu, S. et al. The transcriptional program of sporulation in budding yeast. *Science* **282**, 699-705 (1998).
79. Chu, S. & Herskowitz, I. Gametogenesis in yeast is regulated by a transcriptional cascade dependent on Ndt80. *Mol Cell* **1**, 685-696 (1998).
80. Hepworth, S. R., Friesen, H. & Segall, J. NDT80 and the meiotic recombination checkpoint regulate expression of middle sporulation-specific genes in Saccharomyces cerevisiae. *Mol Cell Biol* **18**, 5750-5761 (1998).
81. Xu, L., Ajimura, M., Padmore, R., Klein, C. & Kleckner, N. NDT80, a meiosis-specific gene required for exit from pachytene in Saccharomyces cerevisiae. *Mol Cell Biol* **15**, 6572-6581 (1995).
82. Sourirajan, A. & Lichten, M. Polo-like kinase Cdc5 drives exit from pachytene during budding yeast meiosis. *Genes Dev* **22**, 2627-2632 (2008).
83. Murakami, H. et al. Multilayered mechanisms ensure that short chromosomes recombine in meiosis. *Nature* **582**, 124-128 (2020).
84. Malone, R. E. et al. Isolation of mutants defective in early steps of meiotic recombination in the yeast Saccharomyces cerevisiae. *Genetics* **128**, 79-88 (1991).
85. Ajimura, M., Leem, S. H. & Ogawa, H. Identification of new genes required for meiotic recombination in Saccharomyces cerevisiae. *Genetics* **133**, 51-66 (1993).
86. Klein, F. et al. A central role for cohesins in sister chromatid cohesion, formation of axial elements, and recombination during yeast meiosis. *Cell* **98**, 91-103 (1999).

87. Møens, P. B. & Pearlman, R. E. Chromatin organization at meiosis. *Bioessays* **9**, 151-153 (1988).
88. Schalbetter, S. A., Fudenberg, G., Baxter, J., Pollard, K. S. & Neale, M. J. Principles of meiotic chromosome assembly revealed in S. cerevisiae. *Nat Commun* **10**, 4795 (2019).
89. Kumar, R., Bourbon, H. M. & de Massy, B. Functional conservation of Mei4 for meiotic DNA double-strand break formation from yeasts to mice. *Genes Dev* **24**, 1266-1280 (2010).
90. Mu, X., Murakami, H., Mohibullah, N. & Keeney, S. Chromosome-autonomous feedback down-regulates meiotic DNA break competence upon synaptonemal complex formation. *Genes Dev* **34**, 1605-1618 (2020).
91. Gray, S., Allison, R. M., Garcia, V., Goldman, A. S. H. & Neale, M. J. Positive regulation of meiotic DNA double-strand break formation by activation of the DNA damage checkpoint kinase Mec1(ATR). *Open Biol* **3**, 130019 (2013).

EXTENDED METHODS

DSB and DC quantifications

DSBs and DCs were quantified with Image gauge software (Fuji). The DSB profile was defined by drawing lanes from the base of the parental band down to the end of the last quantifiable DSB. Background signal was manually removed with a linear subtraction. The signal above the threshold was quantified as a specific signal. DSBs and DCs were quantified as a fraction of the total lane signal observed on gel (which included uncut parental plus all the visible bands). Bands that were observed at time = 0 hours were considered nonspecific and thus not quantified. At the *HIS4*::*LEU2* locus, the fraction of DCs detected with the *LEU2* central probe was multiplied by 3 in order to correct for the fact that only a third of the detected parental DNA signal is derived from the *HIS4*::*LEU2* locus because these strains contain three copies of the *LEU2* gene (*his4X*::*LEU2, leu2*::*hisG* and *nuc1*::*LEU2*). For *ARE1* and *YCR061W* hotspots, the main hotspot (F and N, respectively) was measured with an adjacent probe on the side where there were fewer DSBs prior to the main hotspot, and then corrected by adding the double cuts event present at that region. In the case of *ARE1*, F was measured from the right using *PWP2* probe and the value corrected by adding FI double cuts measured with *ARE1* probe. In the case of *YCR061W*, the main hotspot, N, was measured from the right using *YCR061WII* probe and corrected by adding NO double cuts measured with *YCR061WI* probe. Similarly, at *HIS4*::*LEU2–leu2*::*hisG* loci, quantification of the *leu2*::*hisG* hotspot was measured using *CHA1* probe and corrected by adding *HIS4*::*LEU2–leu2*::*hisG* double-cuts measured with *FRM2* probe. Quantification of the single or double DSB events were displayed as an average of 6, 8 (and occasionally 10) hours after meiosis induction from each repeat. The number of biological repeats is indicated in figure legends. For **Fig 1–2**, measurements from the *NDT80+* background were an average of the data published by Garcia et al (2015) and one and two extra biological replicates developed in this analysis (as specified in figure legends). For **Fig S2–4**, measurements from the *NDT80+* background came only from the data published by Garcia et al (2015).

Calculations of DSB interference

To study DSB interference between two hotspots, the observed frequency of double DSB events that arise at the same molecule (observed DCs) was compared with the expected frequency on the assumption of independence (expected DCs) as described in **Fig S1f–j**. Such expected DC frequency was estimated from multiplication of the frequencies of single DSB events between which DSB interference is studied. To study the strength of interference, the coefficient of coincidence (CoC) was estimated by dividing the observed frequency of DCs by the frequency of expected DCs and subtracting this value from 1 (**Fig S1k**). Positive values close to 1 indicated strong interference, values close to zero indicated independence (no interference) and negative values indicate concerted DSB activity (**Fig S1l**). DSB interference was calculated on a time course basis—from the time 6 and 8 h averaged frequencies—and then averaged across all time courses.

As an example, at *HIS4*::*LEU2*, the frequency of DCs between DSB I and DSB II was measured with a central probe *LEU2* (**Fig 1c,i**). The averaged observed DCs from time 6 and 8 hours, was then compared with the expected frequency of coincident cuts (also averaged time 6 and 8 hours) obtained by multiplying the averaged frequency of DSB I (measured with *MXR2* probe) and DSB II (measured with *HIS4* probe) (**Fig 1c,d-e, l**). Strength of interference was then measured from 1 minus [(Averaged observed DC DSB I–DSB II) / (Averaged expected DC)] frequency in several biological repeats (n = 6 in the case of *NDT80+* background and n = 5 in the case of *ndt80*Δ background) (**Fig 1m**). Using this method, one interference measurement was produced for every repeat and then averaged. Standard deviation and SEM was estimated and a two-tailed T-test performed to measure significant differences between the strains as indicated in the figure legends.

Limitations of the Southern blot and pulsed-field gel electrophoresis techniques

Due to the requirement of multiple gels and the limited resolution of Southern blots and PFGE methods, DSB and DC quantifications are best estimates given the following technical limitations. First, the analysis of many gels analysed in this study indicated that the magnitude of the values varies between both biological and technical repeats depending on gel/blot quality. Second, the strength of the band signal highly influences the quantifications. For instance, weak hotspots are more difficult to characterise than strong ones. Moreover, quantification of DC molecules is challenging in the *TEL1+* background because the level of coincident DSBs is low and generally at or below the detection limit, therefore most of the signal measured is background signal which sometimes can be higher than the calculated expected random frequency (if any of the hotspots is weak) and thus leading to an underestimate of interference strength (e.g. hotspot N and Q; **Fig S3g-h**). Finally, because

the strength of DSB interference is calculated using the division of the observed frequency of double-cut molecules by the frequency expected from independence, the result may be inaccurate when the observed and expected values are close to zero because it produces a disproportionate relative difference that may be artefactual. For example, for this reason the strength of interference was excluded between NO at the *YCR061W* hotspot in the *sae2*Δ and *sae2*Δ *ndt80*Δ (**Fig S3l**).

Another limitation of these techniques is that they only permit an estimate of the number of broken chromatids and not how many times a chromatid has been broken, therefore, quantification of the total frequency of DSBs may be underestimated if the frequency of double events is high (as is the case of *tel1*Δ mutants). Furthermore, the direction and distance from the probe to the hotspot also influences the accuracy of hotspot detection. For example, due to hotspots having a width of 100–300 bp, when the inter-hotspot distance is very short (e.g. hotspots NO, 0.7 kb apart; **Fig S3a**), DC sizes are more variable as a proportion of their length, and the DC probe may also overlap with the DSB positions—both of which may affect their detection on gels.

On the other hand, when the distance between the probe and the measured hotspot is large, the presence of hotspots close to the probe will cause an underestimate of the real frequency of DSBs that are further away. For instance, quantification of the main *ARE1* hotspot “F” slightly differs when measured from the right side of the DSB using *PWP2* probe or from the left with the *TAF2* probe (**Fig S2**). In this example, measurement of F with *TAF2* reported a lower amount of F than *PWP2* probe probably due to the presence of the strong hotspot E prior to F, thus closer to the *TAF2* probe.

The location of the probe is also another factor to consider, especially when a DSB only arises concertedly with another DSB. This seems to be the case of the band smear at *HIS4*::*LEU2* locus detected with *MXR2* and *LEU2* probe but not *HIS4* probe in *sae2*Δ *ndt80*Δ *tel1*Δ mutants (**Fig 1d,i**, red arrow). In fact, the smear detected with the *LEU2* probe indicates the presence of shorter DCs, which would be consistent with either DSB I or DSB II, or both, cutting in different positions within the DSB I–DSB II region. The fact that we can only observe spreading from one side (using *MXR2* probe) indicates that such alternative cutting only happens when DSB I and DSB II cut coincidently, and thus the presence of DSB I will obscure DSB II if measured with *HIS4* probe. Despite these caveats, Southern-blotting techniques are a highly valuable tool to estimate DSB interference at specific loci.

Hotspot identification

Due to the potential variations in the DSB formation displayed in some of the mutants used in this research, a new template of hotspot coordinates was developed in a similar manner to that described in Pan et al (2011) (**Fig S5a**). Hotspots were identified in our baseline *sae2*Δ *ndt80*Δ strains, as well as in other pertinent mutants using a 201 bp Hann window to smooth the Spo11 HpM (hits per million mapped reads) frequency, minimum length of 25 bp and 25 reads and a cut-off of 0.193 HpM. Hotspots separated by < 200 bp were merged and considered as a single hotspot. The new hotspot mask—referred to as the "Neale template"—initially identified a total of 3486 hotspots from a pooled combination of *sae2*Δ *ndt80*Δ and *sae2*Δ *ndt80*Δ *tel1*Δ libraries (3289 were called in *sae2*Δ *ndt80*Δ and 3131 in *sae2*Δ *ndt80*Δ *tel1*Δ) (**Table S4**). 13 of the 3486 hotspots were identified at the rDNA region (position 451640–467844 kb) and therefore removed, reducing the total number of the called hotspots to 3473. From those, a total of 3195 hotspots called in this analysis were also defined by Pan et al (2011) (**Fig S5b**) and 3323 by Mohibullah[58] using the Spo11-oligo maps performed in the Spo11-HA3 and Spo11-ProtA backgrounds respectively (**Fig S5c**), thus validating that most of the hotspots positions we identify are congruent. Moreover, 278 and 150 hotspots, if compared against either Pan's template or Mohibullah's template respectively (**Fig S5b-c**), were exclusively defined in our *sae2*Δ *ndt80*Δ background strains with CC-seq technique, most of which were weak (**Fig S5d**; data not shown). Similarly, 406 and 587 of the specific hotspots only defined by either Pan or Mohibullah, respectively, using the Spo11-oligo technique were also shown to be weak (**Fig S5e-f**). Next, to investigate whether these hotspots were Spo11-specific, hotspots were called in a *sae2*Δ *ndt80*Δ *spo11-Y135F* library identifying a total of 109 potentially false hotspots (**Fig S5g**). For this latter analysis, the cut off was lowered to 0.125 HpM because no hotspots were called with a cut-off of 0.193 HpM. As expected, all the hotspots called in the *sae2*Δ *ndt80*Δ *spo11-Y135F* library were weak (**Fig S5h**). Of those 109 Spo11-nonspecific hotspots, 32 were also called in our new template. Upon visualisation, all 32 hotspots were very weak (data not shown). For detailed information about the mechanics of the scripts see **Hotspot_identification_V1**, **Hotspot_analysis_V1** in **https://github.com/Neale-Lab/Ndt80_LLR**.

Script summary description

Averaging_FullMap_tables_V1: This script averages individual FullMap biological replicates into a combined FullMap where the sum of HpM equals 1 million.

Calculating background reads_V1: This script estimates the percentage of signal registered within the 47 largest genes—regions of presumed Spo11 inactivity—in the *S. cerevisiae* genome as an estimate of the background noise per base pair.

Hotspot_analysis_V1: This script performs pairwise comparisons between datasets to study the degree of overlap, specificity, and density of the identified hotspots (generating Venn diagrams and histograms).

Hotspot_identification_V1: This script identifies position and length of hotspots on single or multiple Spo11-DSB libraries. The total HpM signal is smoothed with a 201 Hann window. A cut-off of 0.193 HpM is then applied to remove the background noise. Hotspots are defined setting a minimum length of 25 bp and a minimum number of reads of 25. Hotspots separated by < 200 bp are merged and considered as a single hotspot. Hotspots are defined in each library separately and then combined to produce a single hotspot template that defines the position of every hotspot identified in the libraries.

Hotspot_Smooth_ratios_V1: This script calculates and represents the hotspot fold changes between two libraries (the NormHpM ratio).

Hotspot_table_V1: This script calculates the HpM and NormHpM signal included within each hotspot. Detailed description of the term heading lists is included in **Hotspot Table Definitions.docx** at **https://github.com/Neale-Lab/Ndt80_LLR**. Briefly, NormHpM refers to the total Spo11 CC-seq signal present in each hotspot (after subtraction of estimated background noise/bp) expressed as a fraction of the total signal in all the hotspot regions. NormHpM values are more robust to differences in library-to-library noise than the raw HpM values (LLR and MJN, unpublished observations).

NormHpM_V1: This script generates DSB maps representing the position and frequency of hotspots (NormHpM or NormHpChr).

Pearson_correlation_V1: This script analyses the correlation between the hotspot strengths of different datasets (NormHpM and NormHpChr Pearson correlation).

Ratio_heatmaps_V1: This script calculates and represents the hotspot fold changes between two libraries (NormHpM) at 50 kb bin intervals on a per chromosome base ranked by chromosome size and centred at the centromere.

Spo11 mapping Totals_V1: This script represents the position and frequency of the Spo11-DSBs signal (Total HpM) along the chromosome.

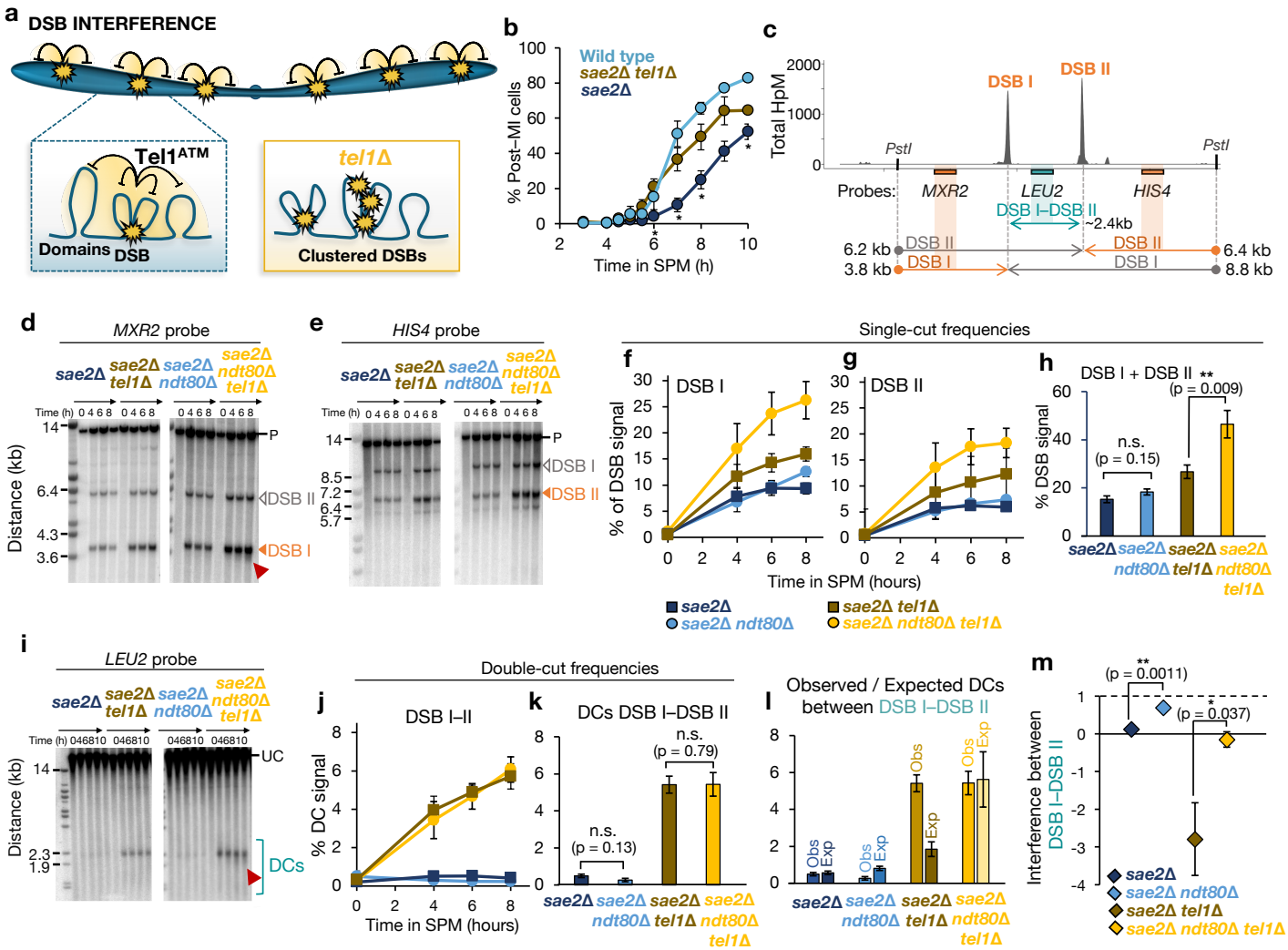

Figure 1. Deletion of *NDT80* ablates negative interference at the *HIS4*::*LEU2* hotspot. a, Schematic representation of the spatial distribution of DSBs by Tel1 DSB interference in the context of the chromosome and the chromosome structure. In the absence of Tel1, the frequency of DSBs increases and DSBs are no longer subject to spatial regulation. **b**, Meiotic nuclear division (MI and MII) kinetics were assessed by counting the appearance of bi-, tri- and tetra-nucleate DAPI-stained cells. At least 100–200 cells were scored for each timepoint after inducing meiosis entry. Averages of n = 2 (Wild type) or n = 3 (*sae2*Δ and *sae2*Δ *tel1*Δ) are represented. Asterisks indicate significant differences ($p < 0.05$) between *sae2*Δ and *sae2*Δ *tel1*Δ cells at the indicated timepoints. **c**, Diagram of the *HIS4*::*LEU2* hotspot showing Spo11-DSB positions as detected by CC-seq in hits per million (HpM; Gittens et al., 2019), and, for Southern blotting experiments, the restriction enzyme sites, probes and size of fragments obtained from each probe. **d–e**, Representative Southern blots of genomic DNA isolated at the specified times hybridised with *MXR2* (**d**), and *HIS4* (**e**) probes. DSBs were marked with a white (non-quantified) or orange (quantified) filled triangle. Red arrows indicated DSB smear on the gels; P, *PstI* digested parental fragment. **f–g**, Quantification of DSB I (**f**), and DSB II (**g**) at the indicated timepoints. **h**, Summary of total DSBs calculated by summing DSB I and DSB II single DSBs (average of 6–8 h time points). **i**, As in **f–g** but with undigested gDNA samples at the indicated timepoints and hybridized with *LEU2* probe. Double cuts (DCs) were highlighted with a blue open bracket. UC, Uncut parental. **j**, Quantification of DC signal at the indicated time points. **k**, Summary of the observed DCs between DSB I and DSB II (average of 6–8 h time points). **l**, Quantification of observed and expected DC frequencies using averaged data from 6–8 h time points in the indicated strains. **m**, DSB interference between DSB I and DSB II calculated for each individual repeat and then averaged (see Extended methods, "Calculation of DSB interference"). Error bars indicate SEM between individual repeats. For statistical analysis, a two-tailed t-test with equal variance samples was performed. n = 6 for *NDT80*+ (4 repeats were used from Garcia et al 2015 and averaged with 2 biological repeats generated in this project) and n = 5 for *ndt80*Δ backgrounds.

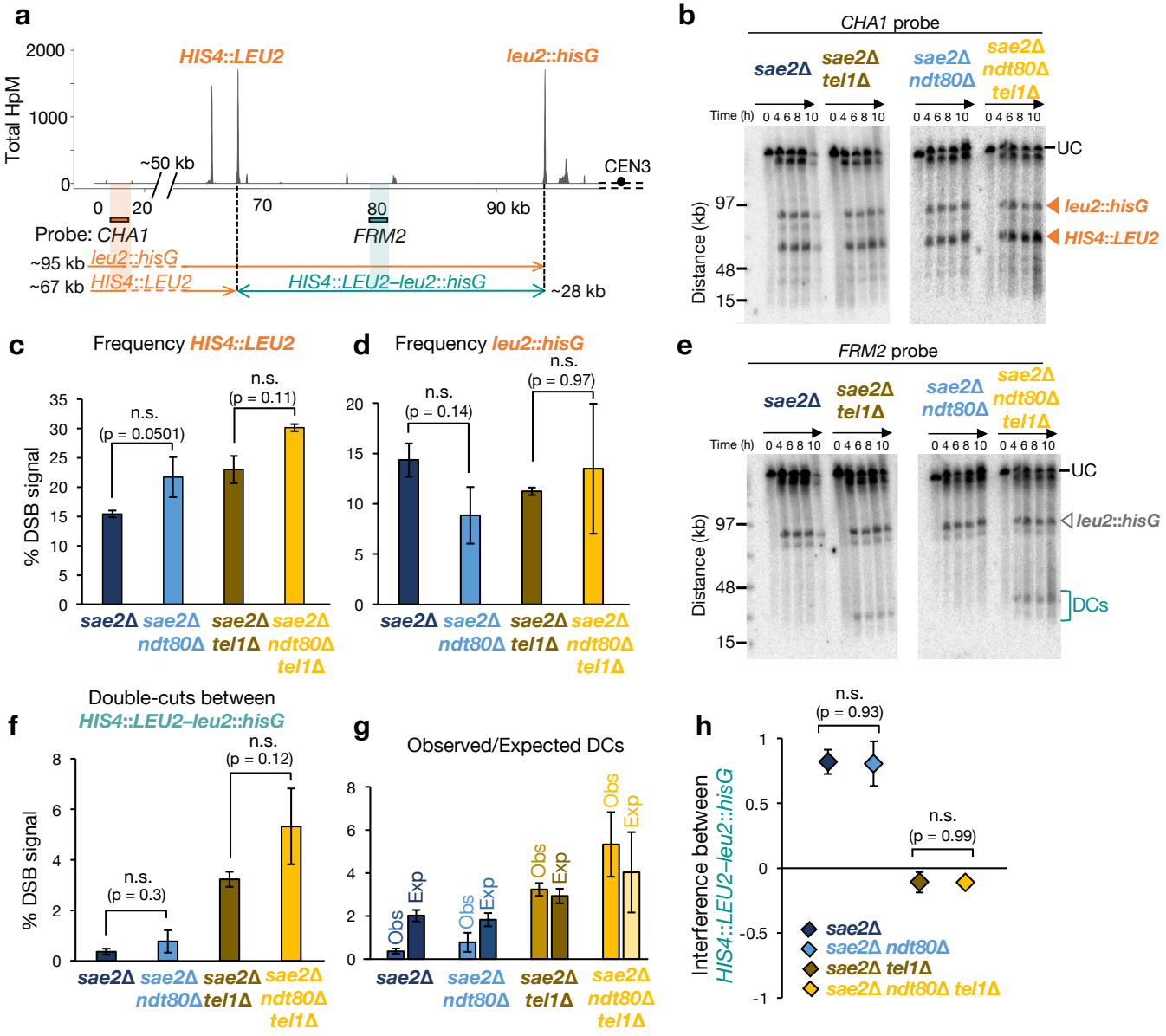

Figure 2. Deletion of *NDT80* does not alter Tel1 DSB interference over medium distances. a, Diagram of the *HIS4*::*LEU2–leu2*::*hisG* region showing positions of the DSBs as measured by CC-seq in hits per million (HpM; Gittens et al., 2019) and, for Southern blotting experiments, the probes and size of fragments obtained from each probe. **b**, Representative Southern blots of agarose-embedded genomic DNA isolated at the specified times separated by PFGE, hybridized with *CHA1* probe. *HIS4*::*LEU2* and *leu2*::*hisG* hotspots are marked with an orange triangle. **c–d**, Average quantification (6 and 8 hours) of *HIS4*::*LEU2* (**c**) and *leu2*::*hisG* (**d**) hotspots. Due to the distance from the *CHA1* probe, the *leu2*::*hisG* DSB frequency is calculated by adding on the frequency of DCs as measured with the *FRM2* probe (as in Garcia et al 2015). **e**, As in (**b**) but hybridized with *FRM2* probe. Double cuts (DCs) between *HIS4*::*LEU2—leu2*::*hisG* are marked with a blue open bracket. UC, Uncut parental. **f**, Average quantification (6 and 8 hours) of DCs between *HIS4*::*LEU2—leu2*::*hisG*. **g**, Quantification of observed and expected DC frequencies using averaged data from 6–8 h time points in the indicated strains. **h**, DSB interference between *HIS4*::*LEU2* and *leu2*::*hisG* hotspots was calculated for each individual repeat and then averaged (see Extended methods, “Calculation of DSB interference”). Error bars indicate SEM between individual repeats. For statistical analysis, a two-tailed t-test with equal variance samples was performed. n=5 for *NDT80*$^{+}$ (4 repeats were used from Garcia et al 2015 and averaged with 1 biological repeat generated in this project) and n=2 for *ndt80Δ* backgrounds.

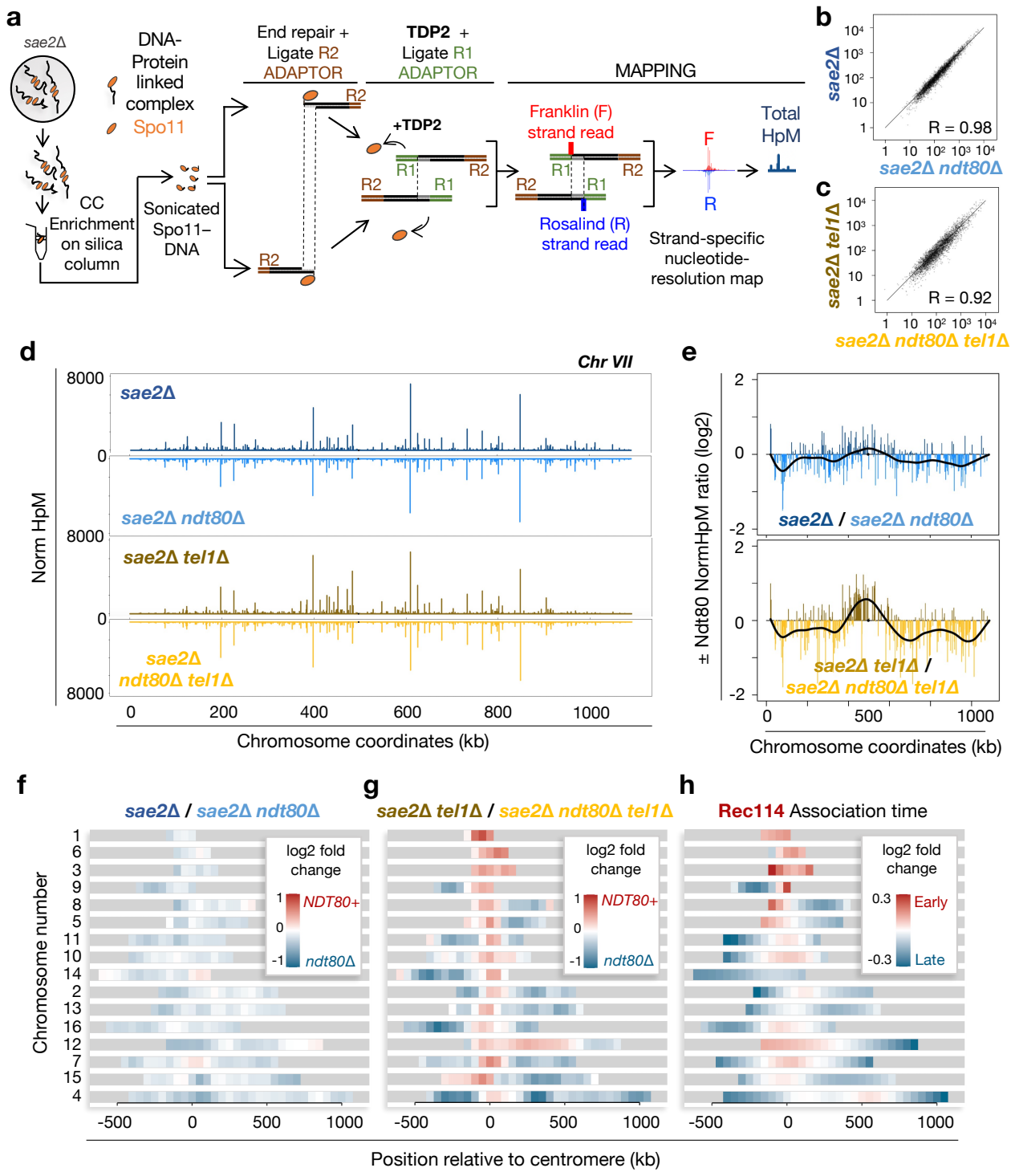

Figure 3. Deletion of *NDT80* influences the distribution of DSBs at a genome-wide scale. **a**, Schematic of the genome-wide CC-seq Spo11-DSB mapping technique (see Extended methods). **b–c**, Pearson correlation of Spo11 hotspot strengths (NormHpM) in the presence and absence of Ndt80 in *TEL1*+ (**b**) and *tel1*Δ cells (**c**). **d**, Visualization of the relative Spo11 hotspot intensities on chromosome VII in the indicated strains. **e**, Ratio of relative Spo11 hotspot intensities ±*NDT80* on chromosome VII in the presence (upper panel) and absence (lower panel) of Tel1. Values above zero indicate a higher DSB frequency in the presence of Ndt80 and below zero a higher DSB frequency in the absence of Ndt80. Fold change was smoothed to highlight the spatial trend effect of *NDT80* deletion (black line). Other chromosomes are presented in **Fig S6**. **f–g**, Heat maps representing ±Ndt80 effect in the presence (**f**) and absence of Tel1 (**g**). Log2 ratio of relative hotspot strengths ±*NDT80* was binned into 50 kb intervals and plotted centred at the centromere and ranked by chromosome size. **h**, Pattern of relative Rec114 association time, reported by Murakami et al (2020) and presented as in **f-g**.

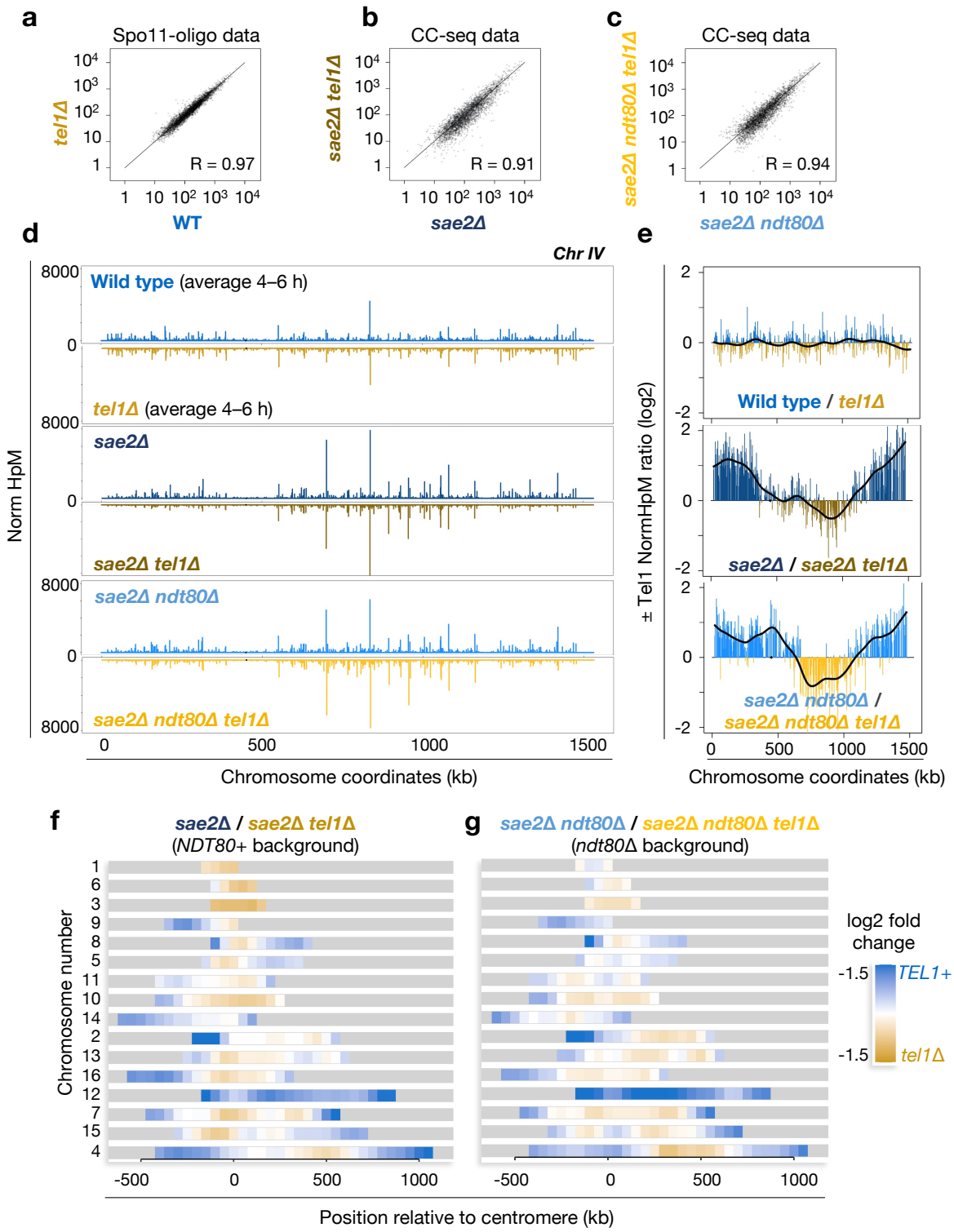

Figure 4. Tel1-dependent genome-wide effect on DSB distribution. a–c, Pearson correlation of Spo11 hotspot strengths (NormHpM) in the presence and absence of Tel1 in *SAE2*+ (Spo11-oligo maps; Mohibullah and Keeney, 2017) (**a**), and in CC-seq maps in *sae2*Δ (**b**) and *sae2*Δ *ndt80*Δ (**c**) strains. **d**, Visualization of the relative Spo11 hotspot intensities on chromosome IV in the indicated strains. **e**, Ratio of relative Spo11 hotspot intensities ±*TEL1* on chromosome IV in *SAE2*+ cells (Spo11-oligo data; upper panel) and in CC-seq maps in the presence (middle panel) and absence (lower panel) of Ndt80. Values above zero indicate a higher DSB frequency in the presence of Tel1 and below zero a higher DSB frequency in the absence of Tel1. Fold change was smoothed to highlight the spatial trend caused by *TEL1* deletion (black line). Other chromosomes are presented in **Fig S7**. **f–g**, Heat maps of CC-seq data (*sae2*Δ) representing the ±Tel1 effect in the presence (**f**) and absence of Ndt80 (**g**). Log2 ratio of relative hotspot strengths ±*TEL1* was binned into 50 kb intervals and plotted centred on the centromere and ranked by chromosome size.

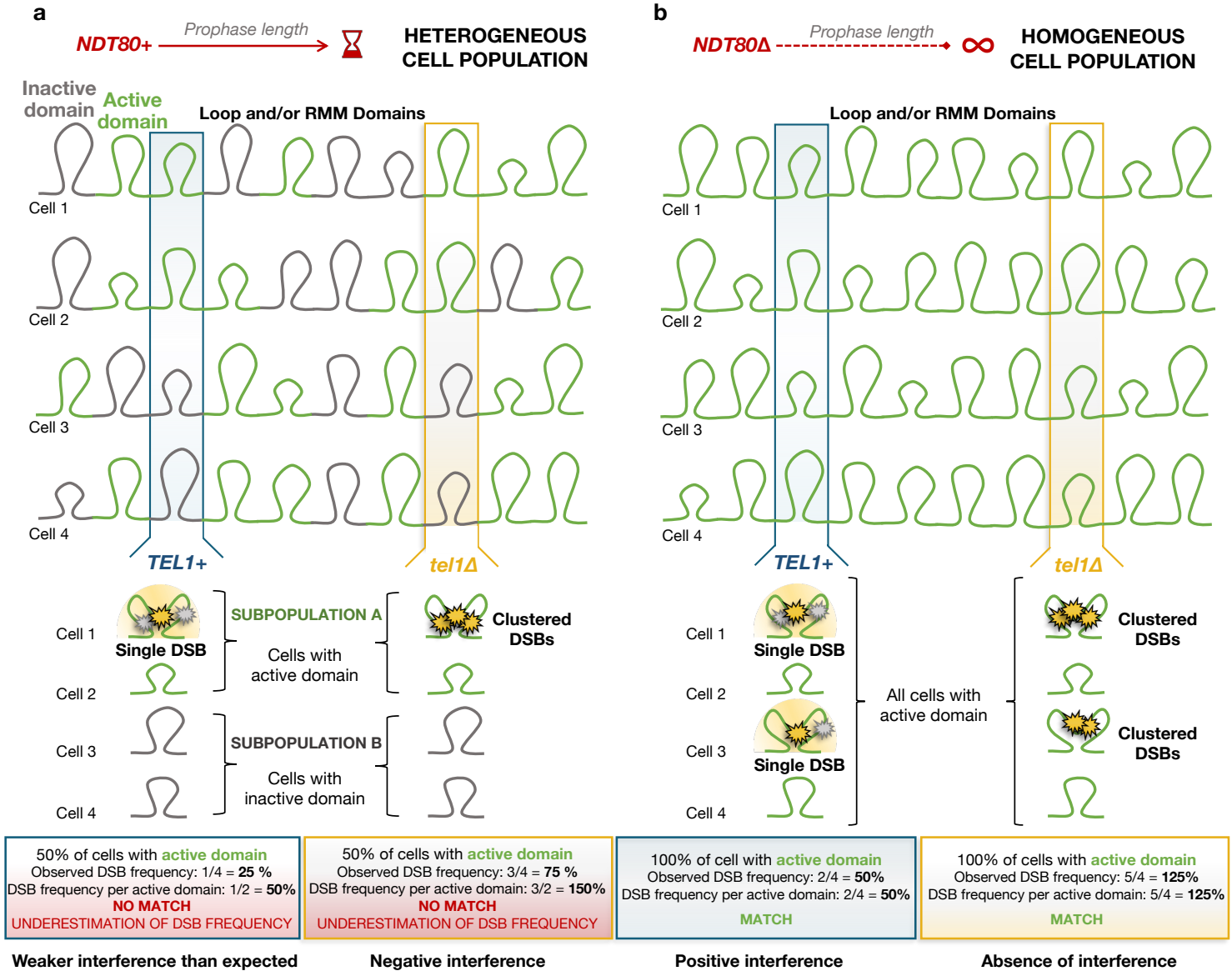

Figure 5. Meiotic prophase length homogenises the potential of forming active domains in which DSB formation may arise. **a**, Schematic representation of a heterogeneous mixture of cells with active and inactive domains with differing potential for DSB formation in *NDT80+* cells. The formation of such active/inactive subdomains will bias the measurement of DSB frequency leading to lower-than-expected calculations of DSB interference. In the presence of Tel1, underestimation of the DSB probability within the active domains would generate weaker interference than expected, whereas, in the absence of Tel1 (*tel1Δ*), the lack of local DSB inhibition will cause efficient coincident cutting (DSB clustering) in the fraction of cells with the active domain, causing negative interference. In both examples we represent a situation in which 50% of the assayed population of cells—here represented with just four chromatids for simplicity—have the domain active at the tested region. **b**, We propose that deletion of *NDT80* extends the length of the meiotic prophase homogenising the potential for domains to be activated and allowing a more accurate detection of DSB frequency per active domain. In the presence of Tel1, DSBs will arise evenly across the genome—leading to detection of positive interference, whereas in *tel1Δ* cells, the lack of negative inhibition will lead to detection of no interference. In both examples we represent a situation in which 100% of the assayed population of cells—here represented in four chromatids for simplicity—have the domain active at the tested region. Although Spo11-DSB formation arises in the context of a maturing loop-axis chromosome structure organised by cohesin, and contains chromatin loops that are within the size range (in *S. cerevisiae*) over which we infer activation to occur (<15 kb), such active domains may simply coincide with, and co-occur alongside loop formation, but not necessarily depend upon their existence, instead being driven by the assembly of pro-DSB factors such as Rec114, Mei4 and Mer2 (RMM; see discussion for further details).

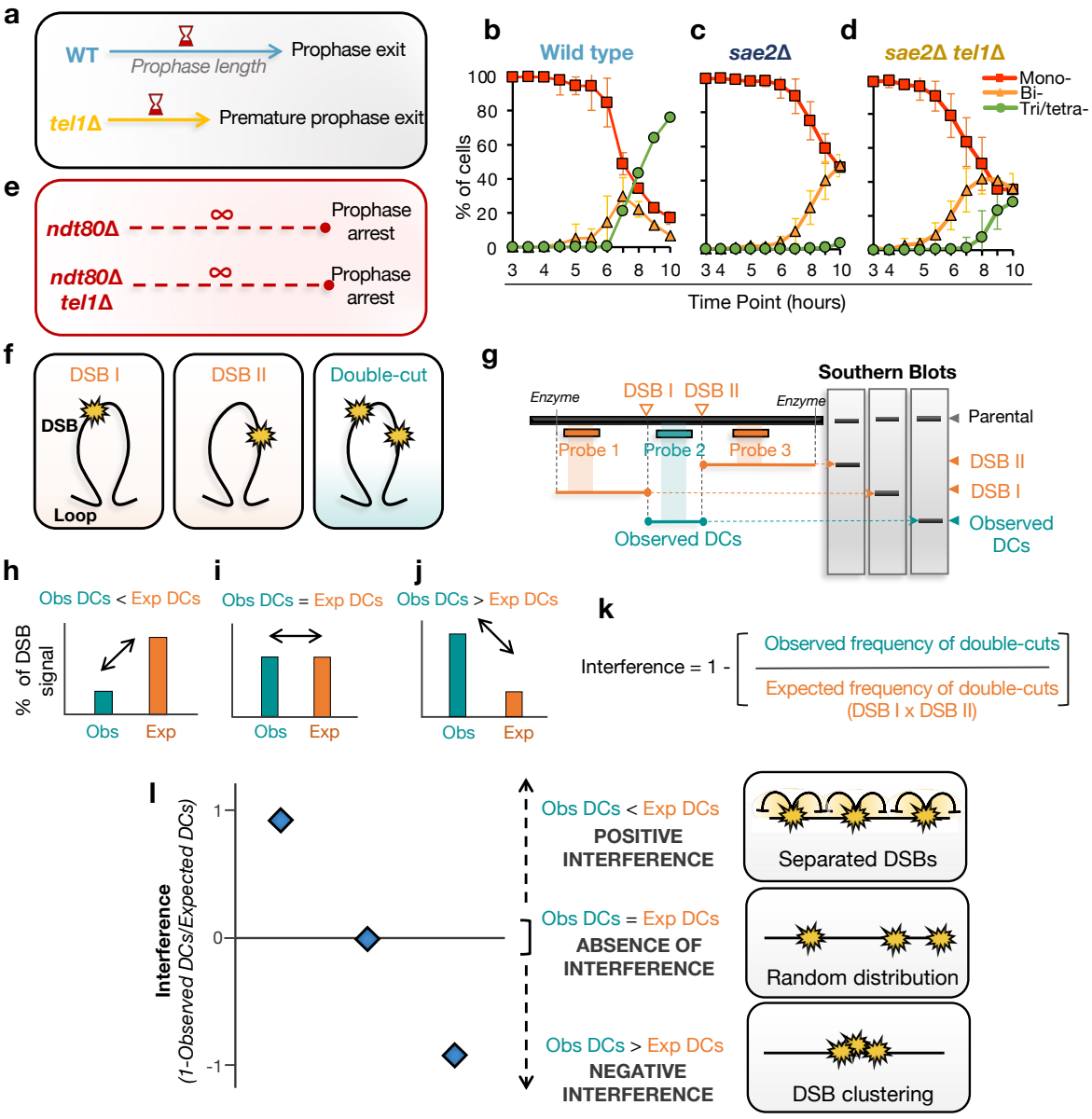

Supplementary Figure 1. Calculating DSB interference. **a**, Schematic representation of the potential prophase length differences between ± Tel1. In the absence of Tel1, the checkpoint may be down-regulated resulting in a reduction of the meiotic prophase length. **b–d**, Meiotic nuclear division (MI and MII) kinetics showing the individual profiles of mono- bi-, tri/tetra-nucleate DAPI-stained cells for Wild type (**b**), *sae2*Δ (**c**) and *sae2*Δ *tel1*Δ (**d**). Summary of bi- tri- and tetra- previously presented in **Fig 1b**. **e**, Schematic representation of the expected effect of *ndt80*Δ mutation. Removal of *NDT80* generates cell cycle arrest in late meiotic prophase I and therefore equalizes the length of meiotic prophase regardless of the presence or absence of Tel1. **f–l**, Simplified schematics of the Southern blot method used to study DSB interference at specific loci. **f**, Diagram representing a theoretical loop domain containing two hotspots (DSB I and DSB II) that can arise independently or coincidently (double-cut, DC). **g**, Diagram representing the position of the probes and fragments that would be used to detect each of the single DSBs or the coincident double-cut by Southern blotting techniques in this theoretical scenario. The probability of both DSBs arising from independence (Expected double-cuts), can be estimated by measuring and multiplying the single DSB event frequencies. **h–j**, Three possible scenarios can result from comparing the estimated expected DC frequency with the observed DC frequency. The expected DC frequency can be higher (**h**), similar (**g**) or lower (**j**) than the observed DC frequency. **k**, The strength of interference can be calculated by subtracting subtracting from 1, the coefficient of coincidence (CoC)—which is estimated by dividing the observed frequency of DCs by the frequency expected on the assumption of independence. **l**, Interference values close to 1 indicate positive interference and thus separate DSB events. Interference values close to zero indicate absence of interference, thus random distribution of DSBs. Whereas interference values below 0 indicate negative interference and thus concerted DSB activity (DSB clustering).

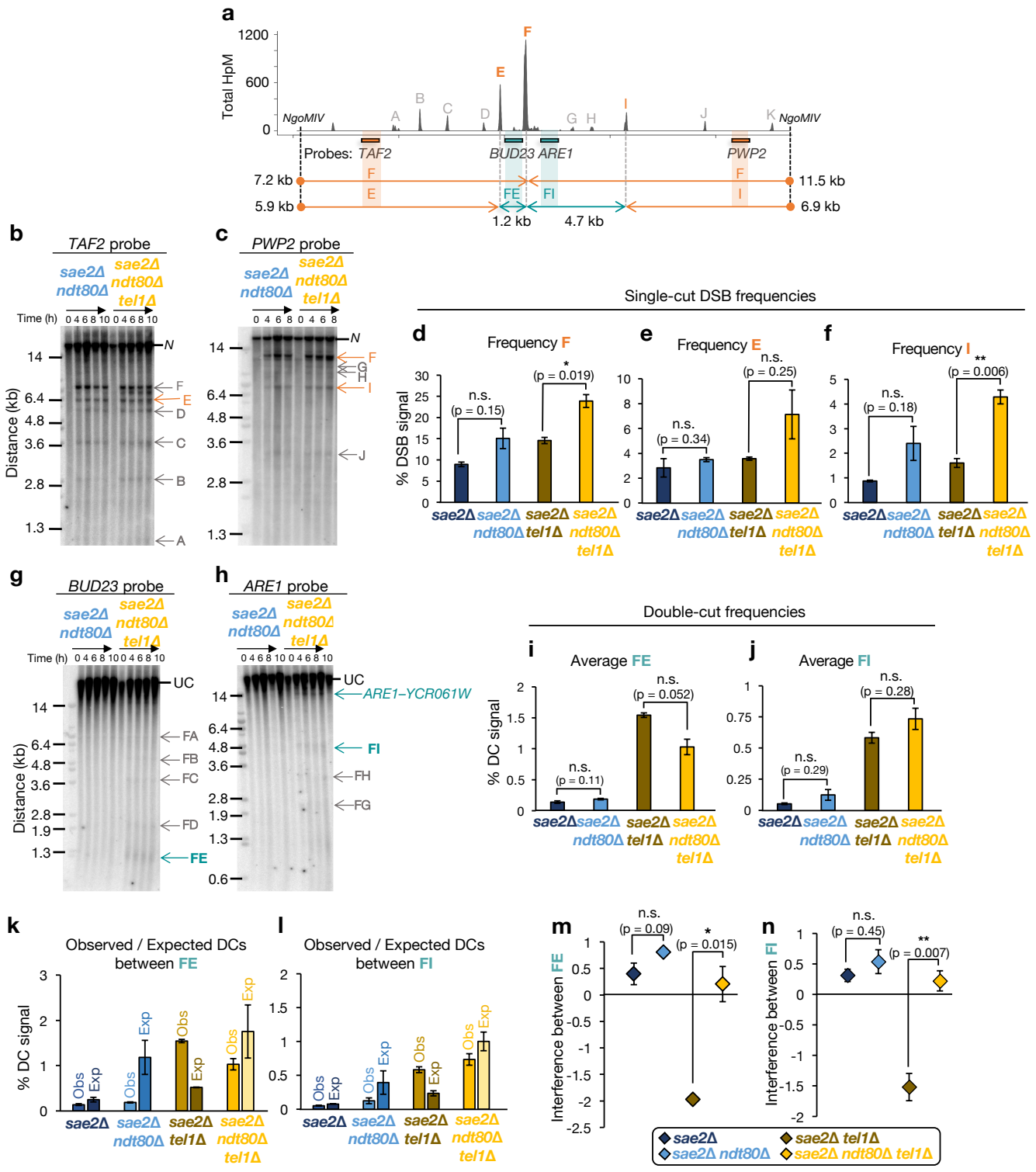

Supplementary Figure 2. Deletion of *NDT80* ablates negative interference at the *ARE1* hotspot. a, Diagram of the *ARE1* hotspot showing Spo11-DSB positions as detected by CC-seq in hits per million (HpM; Gittens et al., 2019), and, for Southern blotting experiments, the restriction enzyme sites, probes and size of fragments obtained from each probe. DSB interference was only measured between the main hotspot F–E and F–I. **b–c**, Representative Southern blots of genomic DNA isolated at the specified times hybridised with *TAF2* (**b**), and *PWP2* (**c**) probes. Quantified DSBs were marked in orange and not-quantified DSBs in grey. N, *NgoMIV* digested parental fragment. **d–f**, Quantification of F (**d**), E (**e**) and I (**e**) hotspots (average of 6–8 h time points). Estimation of F was corrected by adding on FI double-cuts measured with *ARE1* probe. **g–h**, As in **b–c** but with undigested gDNA samples at the indicated timepoints and hybridized with *BUD23* (**g**) and *ARE1* (**h**) probes. Quantified DCs were marked in blue and not-quantified DSBs in grey. UC, Uncut parental. **i–j**, Quantification of DC signal between FE (**i**) and FI (**j**) (average of 6–8 h time points). **k–l**, Quantification of observed and expected DC frequencies between FE (**k**) and FI (**l**) using averaged data from 6–8 h time points in the indicated strains. **m–n**, DSB interference between FE (**m**) and FI (**n**) calculated for each individual repeat and then averaged (see Extended methods, "Calculation of DSB interference"). Error bars indicate SEM between individual repeats. For statistical analysis, a two-tailed t-test with equal variance samples was performed. n = 2 for *NDT80+* (from Garcia et al 2015) and n = 3 for *ndt80Δ* backgrounds.

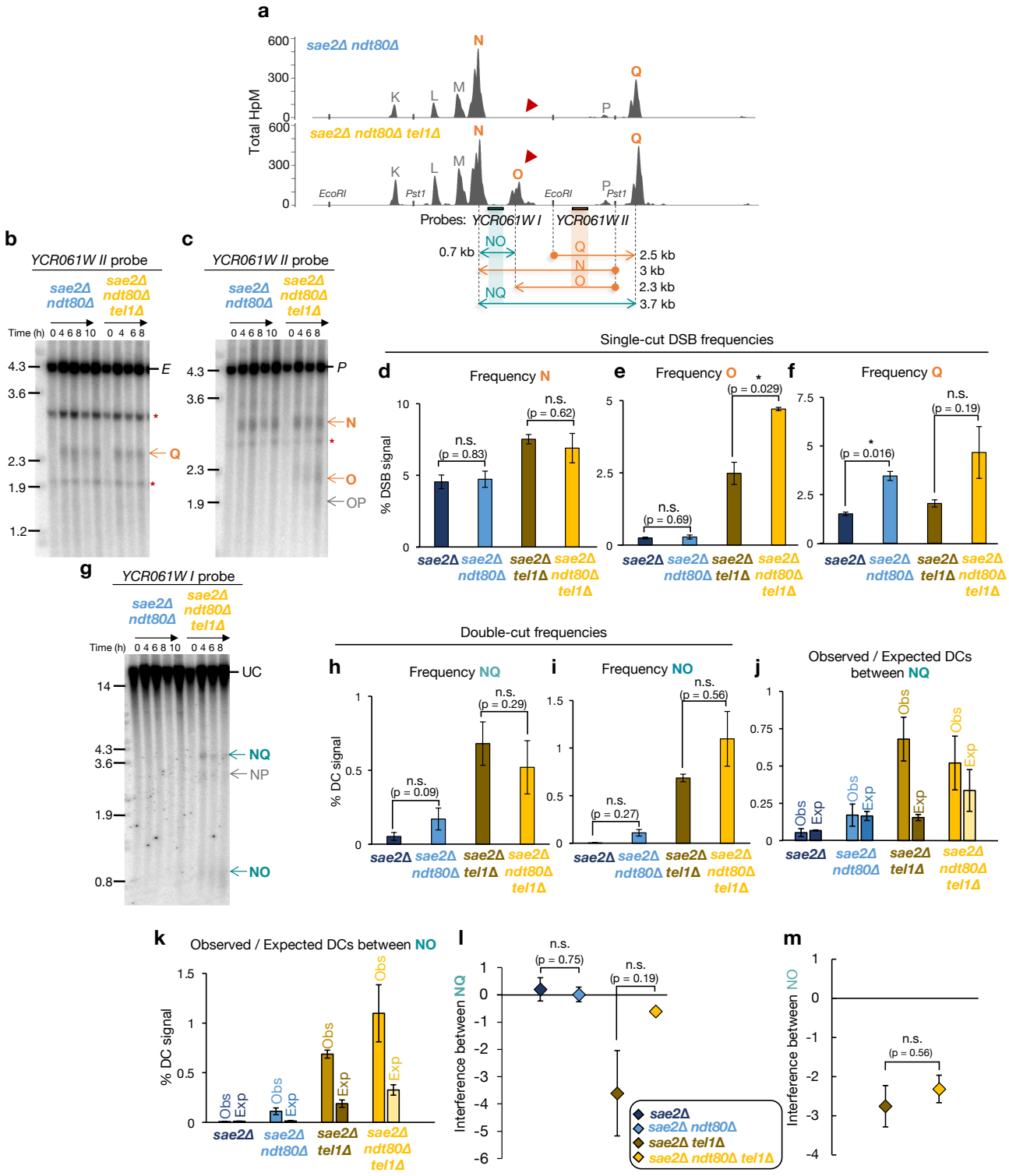

Supplementary Figure 3. Interference at the *YCR061W* hotspot. **a**, Diagram of the *YCR061W* hotspot showing Spo11-DSB positions as detected by CC-seq (Gittens et al., 2019) in hits per million (HpM) and, for Southern blotting experiments, the restriction enzyme sites, probes and size of fragments obtained from each probe. DSB interference was only measured between the main hotspots N–O and N–Q. **b–c**, Representative Southern blots of genomic DNA isolated at the specified times hybridised with *YCR061W II* probe. E, *EcoRI* digested parental fragment (**b**) and P, *PstI* digested parental fragment (**c**) Quantified DSBs were marked in orange and not-quantified DSBs in grey. N, *NgoMIV* digested parental fragment. **d–f**, Quantification of N (**d**), O (**e**) and Q (**e**) hotspots (average of 6–8 h time points). Estimation of N was corrected by adding on NO DCs measured with the *YCR061W I* probe. **g**, As in **b–c** but with undigested gDNA samples at the indicated timepoints and hybridized with the *YCR061W I* probe. Quantified DCs were marked in blue and not-quantified DSBs in grey. UC, Uncut parental. **h–i**, Quantification of DC signal between NQ (**h**) and NO (**i**). **j–k**, Quantification of observed and expected DC frequencies between NQ (**j**) and NO (**k**) using averaged data from 6–8 h time points in the indicated strains. **l–m**, DSB interference between NQ (**l**) and NO (**m**) calculated for each individual repeat and then averaged (see Extended methods, "Calculation of DSB interference"). Error bars indicate SEM between individual repeats. For statistical analysis, a two-tailed t-test with equal variance samples was performed. n = 2 for *NDT80+* (from Garcia et al 2015) and for *ndt80Δ* backgrounds.

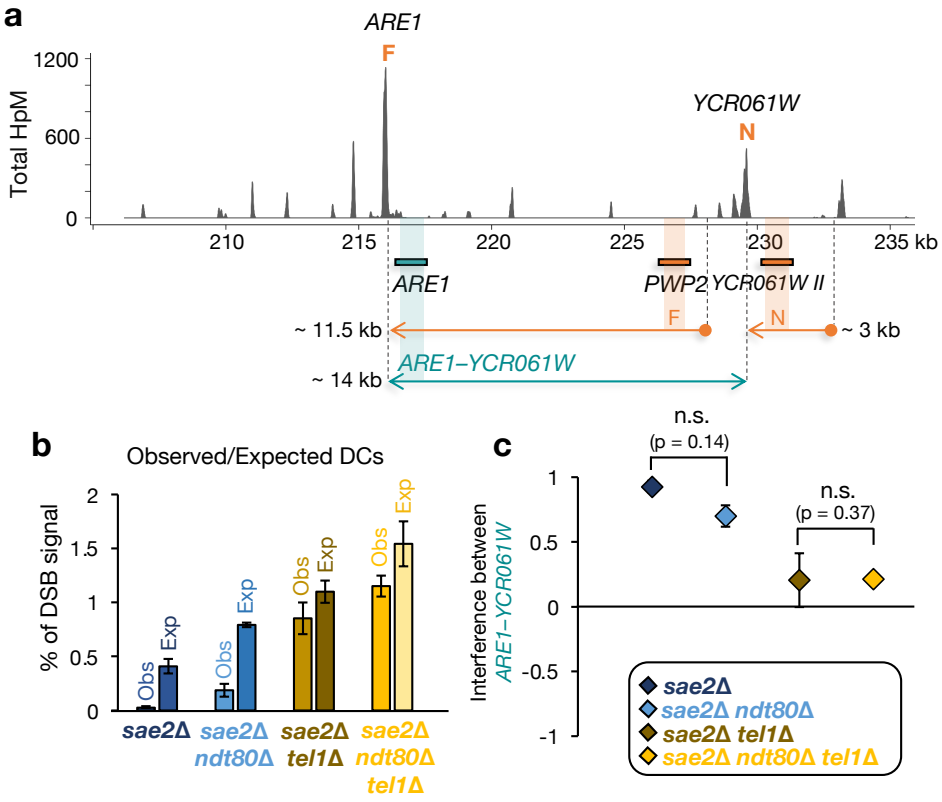

Supplementary Figure 4. Deletion of *NDT80* does not alter Tel1 DSB interference over medium distances (*ARE1–YCR061W*). **a**, Diagram of the region comprised between *ARE1* and *YCR061W* hotspots showing Spo11-DSB positions as detected by CC-seq in hits per million (HpM; Gittens et al., 2019), and, for Southern blotting experiments, the probes and size of fragments obtained from each probe. Quantification of F and N was obtained from **Fig S2c**, and **Fig S3c**, respectively. Quantification of DCs between *ARE1–YCR061W* was obtained from **Fig S2h**. **b**, Quantification of observed and expected DC frequencies between *ARE1–YCR061W* using averaged data from 6–8 h time points in the indicated strains. **c**, DSB interference between *ARE1–YCR061W* hotspot calculated for each individual repeat and then averaged (see Extended methods, "Calculation of DSB interference"). Error bars indicate SEM between individual repeats. For statistical analysis, a two-tailed t-test with equal variance samples was performed. n = 2 for *NDT80+* (from Garcia et al 2015) and for *ndt80Δ* backgrounds.

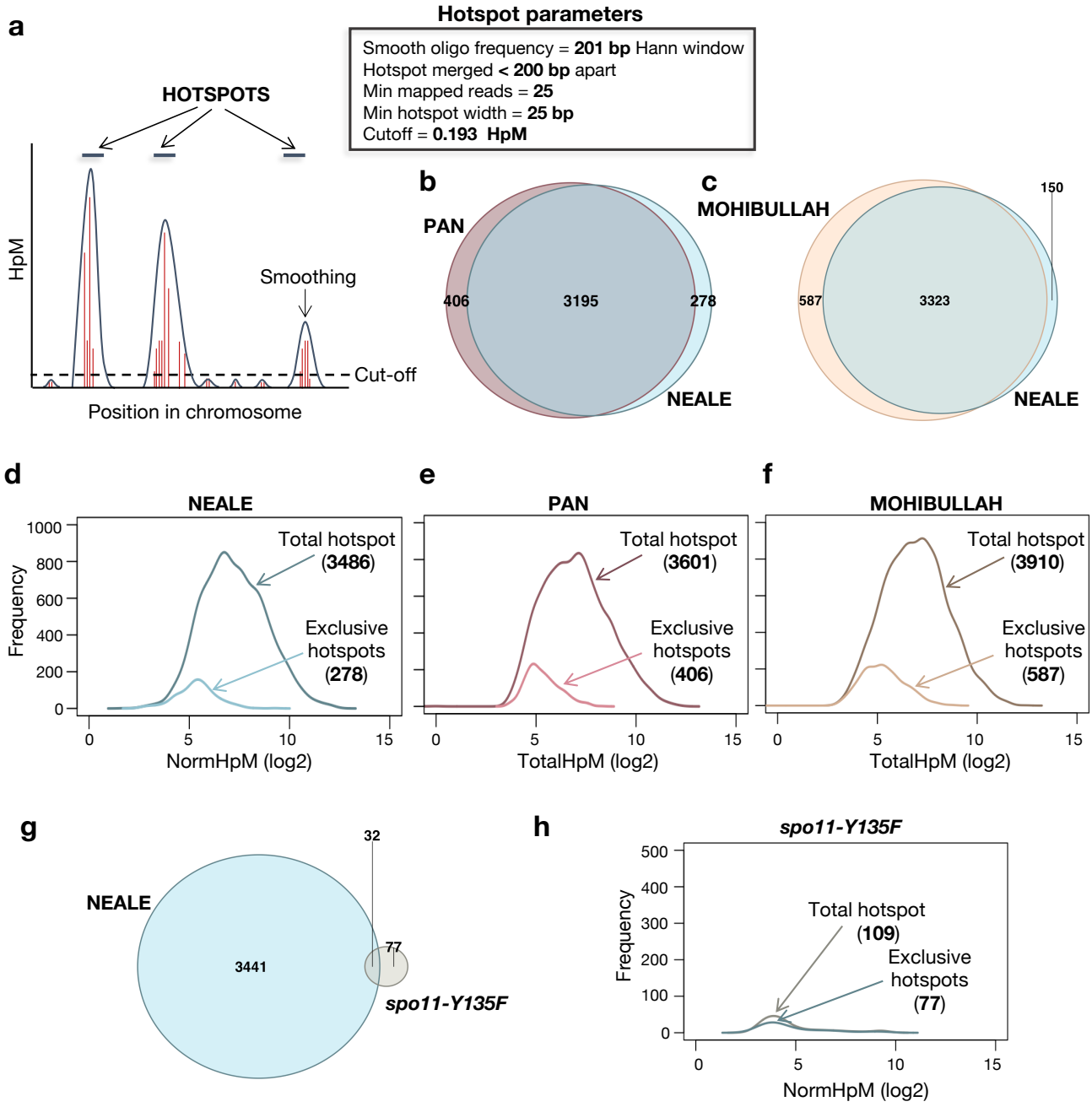

Supplementary Figure 5. Identification of Spo11 hotspots. a, Diagram representing the hotspot calling method (see Extended method, "Hotspot identification"). The frequency of HpM was smoothed using a 201 bp Hann window with a minimum length of 25 bp, 25 reads and a cut-off of 0.193 HpM to filter for noise signal. Hotspots separated by < 200 bp were merged and considered as a single hotspot. In this study, hotspots were identified from a pooled combination of *sae2Δ ndt80Δ* and *sae2Δ ndt80Δ tel1Δ* (Neale template). **b–c**, Venn diagrams of overlap between hotspots identified in this study by CC-seq (Neale) and hotspots identified by Spo11oligo mapping by Pan et al. 2011 (**b**) or Mohibullah et al 2017 (**c**). **d–f**, Distribution of hotspot frequency for the total and exclusive hotspots identified by Neale vs Pan (**d**), Pan vs Neale (**e**) and Mohibullah vs Neale (**f**). **g**, Venn diagrams of overlap between hotspots identified in the Neale template and the non-specific hotspots identified in the *spo11-Y135F* strain. The cut-off for hotspot calling in the *sae2Δ ndt80Δ spo11-Y135F* mutant was lowered to 0.125 HpM. **h**, as in **d–f** but Neale vs *sae2Δ ndt80Δ spo11-Y135F* template.

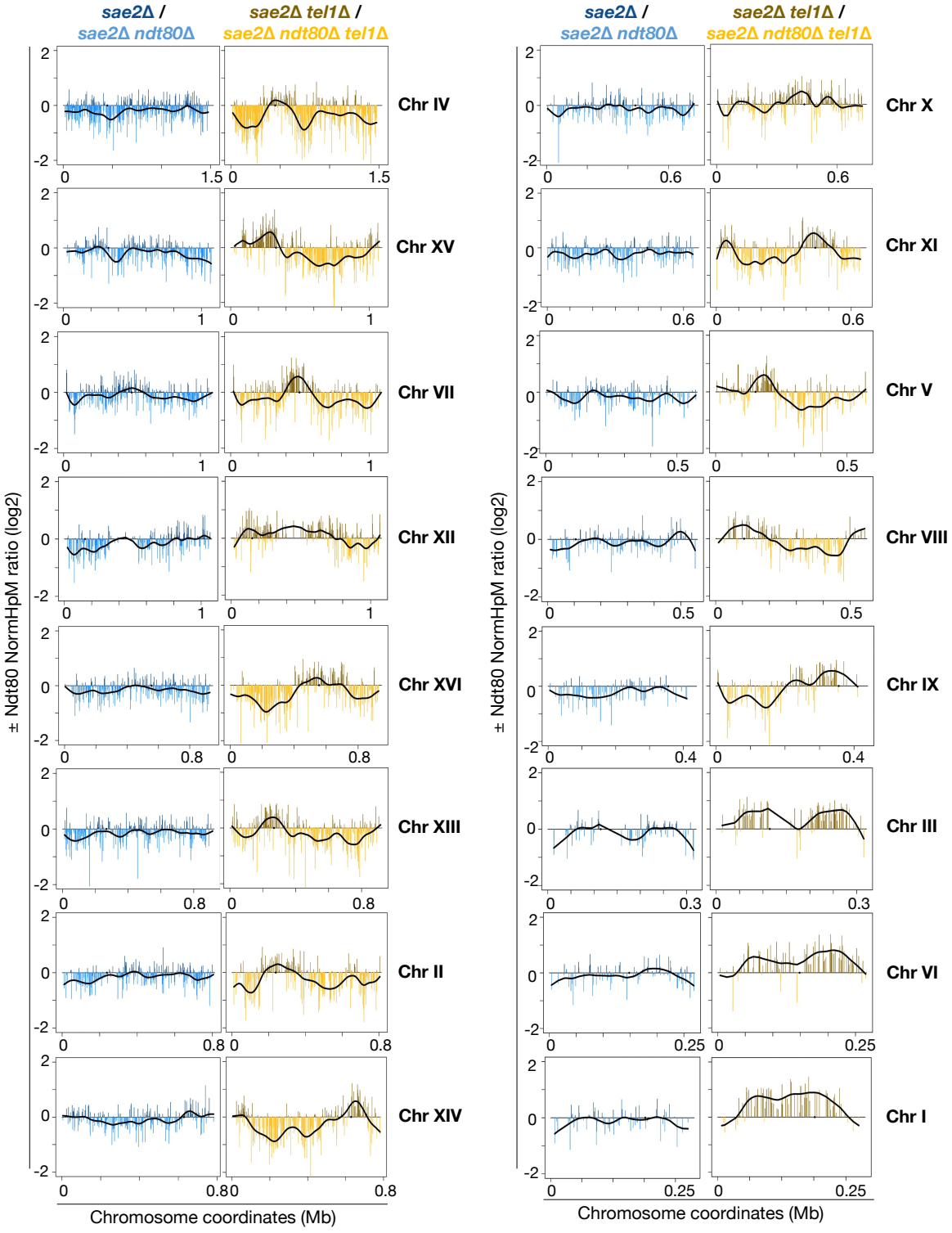

Supplementary Figure 6. Ndt80 genome-wide effect on a per chromosome basis. Log2 ratio of relative Spo11 hotspot intensities ±*NDT80* on all chromosomes in the presence (left panel) and absence (right panel) of Tel1. Values above zero indicate a higher DSB frequency in the presence of Ndt80 and below zero a higher DSB frequency in the absence of Ndt80. Fold change was smoothed to highlight the spatial trend effect of *NDT80* deletion (black line).

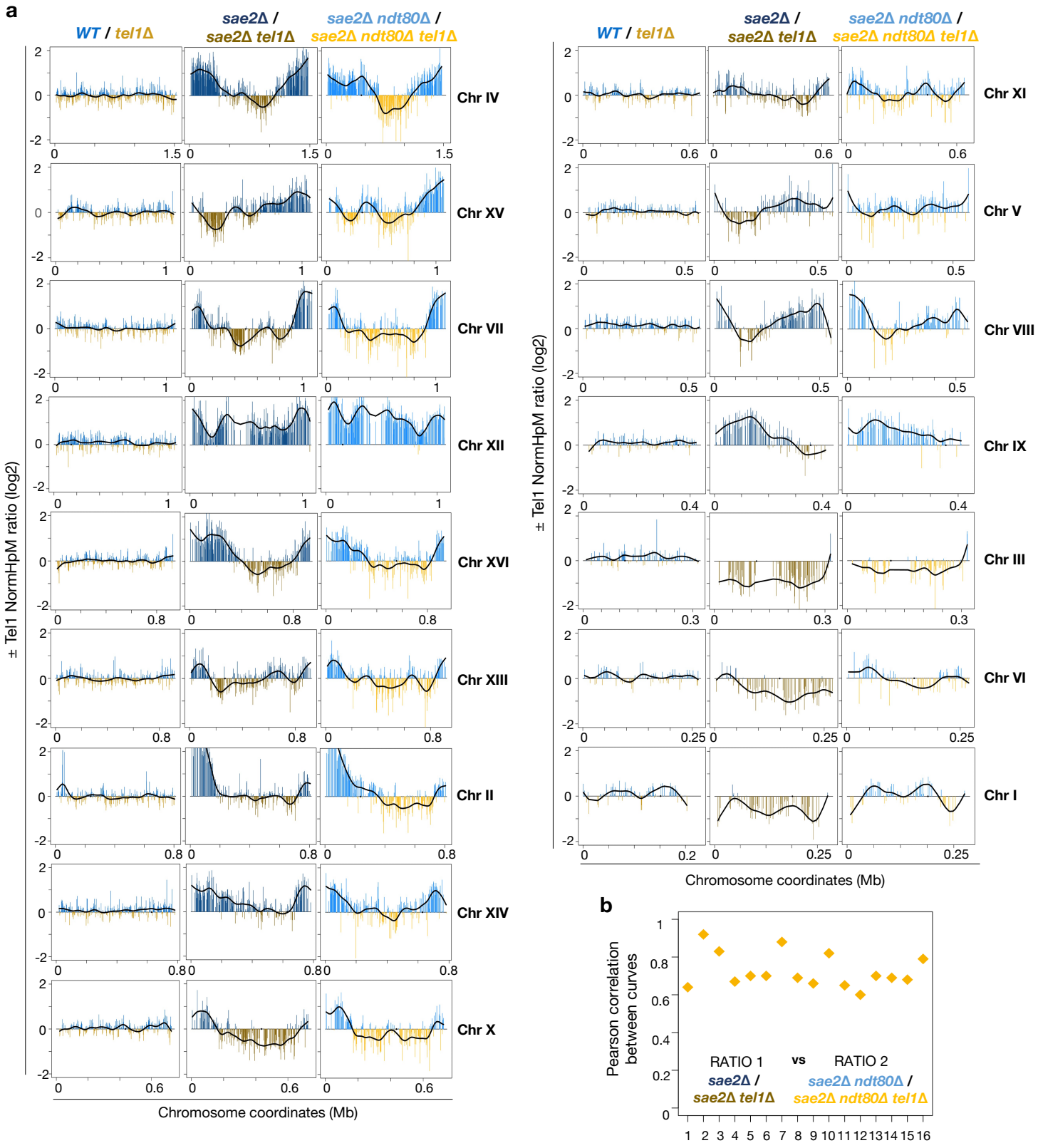

Supplementary Figure 7. Tel1 genome-wide effect on a per-chromosome basis. a, Log2 ratio of relative Spo11 hotspot intensities ±*TEL1* on all 16 chromosomes in *SAE2*+ cells with Spo11-oligo technique (left panel) and *sae2*Δ cells with CC-seq technique in the presence (middle panel) and absence (right panel) of Ndt80. Values above zero indicate a higher DSB frequency in the presence of Tel1 and below zero a higher DSB frequency in the absence of Tel1. Fold change was smoothed to highlight the spatial trend caused by *TEL1* deletion (black line). **b,** Plot showing the Pearson correlation between ± Tel1 smoothed ratios in the presence (RATIO 1) and absence of Ndt80 (RATIO 2).

Table S1. *S. cerevisiae* strains used in this study

STRAIN	NAME	GENOTYPE
MJ315	*sae2Δ*	*MATa/alpha ho::LYS2/', lys2/', ura3/', arg4-nsp/', leu2::hisG/', his4X::LEU2/', nuc1::LEU2/', sae2Δ::KanMX6/'*
VG402	*sae2Δ tel1Δ*	*MATa/alpha ho::LYS2/", lys2/", ura3/", arg4-nsp/", leu2::hisG,/" his4X::LEU2/", nuc1::LEU2/", sae2Δ::KanMX4/", tel1Δ::HphMX4/"*
MJ962	*sae2Δ ndt80Δ*	*MATa/alpha ho::LYS2/", lys2/", ura3/", arg4-nsp/", leu2::hisG,/" his4X::LEU2/", nuc1::LEU2/", sae2Δ::KanMX6/", ndt80Δ::LEU2/''*
MJ965	*sae2Δ ndt80Δ tel1Δ*	*MATa/alpha ho::LYS2/", lys2/", ura3/", arg4-nsp/", leu2::hisG,/" his4X::LEU2/", nuc1::LEU2/", sae2Δ::KanMX6/", ndt80Δ::LEU2/'', tel1Δ::HYG/''*
GB21	*sae2Δ ndt80Δ spo11-Y135F*	*MATa/alpha ho::LYS2/", lys2/", ura3/", arg4-nsp/", leu2::hisG,/" his4X::LEU2/", sae2Δ::KanMX6/", ndt80Δ::LEU2/'', spo11(Y135F)::KanMX4/"*

Table S2. Oligonucleotides used in this study for Southern Blots

PROBE	CHR	PRIMERS	DIGESTION	COMMENTS
CHA1	Chr III	CHA1_F@-9: ACCAGCGAGATGTCGATAGTCTAC CHA1_R@+1052: TCTGGAAATATGAAATTGTCAGCG	*NA*	Quantification of *HIS4::LEU2* and *leu2::hisG* hotspots
FRM2	Chr III	FRM2_F@+27: GCTATTACAAACCGTCGTACCATC FRM2_R@+645: CATCGCTGAGGTATCATTACTTCAT	*NA*	Quantification of double-cuts between *HIS4::LEU2* and *leu2::hisG* hotspots
LEU2	Chr III	LEU2_F: ATATACCATTCTAATGTCTGC LEU2_R: AAGGATTTTCTTAACTTCTTCGGCG	*NA*	Quantification of double-cuts between DSB I–DSB II at *HIS4::LEU2* hotspot
HIS4	Chr III	HIS4LH_F: CTACTGGAAATCCTTTGGGATCAACCC HIS4LH_R: CTTGGGTCCAGGTAATCAATTTGTGACTG	*PstI*	Quantification of DSB II at *HIS4::LEU2* hotspot
MXR2	Chr III	HIS4_F@+5170: CGTGAAGTGGAACGATGCCC HIS4_R@+5493: GCAACTGTTTCCAGCCTTCACC	*PstI*	Quantification of DSB I at *HIS4::LEU2* hotspot
BUD23	Chr III	BUD23_F@+1: ATGTCACGTCCTGAGGAGTTGG BUD23_R@+800: GTGAACTTGGAGTCCTTCGCAAC	*NA*	Quantification of double-cuts between the main *ARE1* (F) and hotpots to the left
ARE1	Chr III	ARE1_F@+54: ACTCAATTCCGCAGAAGCCA ARE1_R@+715: TTGCCAAGTCCAACATTGCG	*NA*	Quantification of double-cuts between *ARE1* (F) and hotpots to the right Quantification of double-cuts between *ARE1* and *YCR061W* hotspots
TAF2	Chr III	TAF2_F@+23: CCACTCCTAGAGCCATTGTTAG TAF2_R@+693: TCATCAAGCAAATCGACACATGG	*NgoMIV*	Quantification of adjacent hotspots to the left of *ARE1* (F)
PWP2	Chr III	PWP2_F@+35: GTACGGTCTACAGGCAAGGTAAC PWP2_R@+815: TTGCTGGATGGAAGGTGACACAC	*NgoMIV*	Quantification of main *ARE1* (F) and adjacent hotspots to the right of ARE1
YCR061W I	Chr III	YCR061W_F@+58: CCCATGATGACATGGACATGGAC YCR061W_R@+884: GGTATGTCTTGAGGAAGCAGAGG	*NA*	Quantification of double-cuts between *YCR061W* (N) and hotpots on the right of *YCR061W*
YCR061W II	Chr III	YCR061WII_R@+2176: TCAGAGAGAACCTCCAGTAGAGTC YCR061WII_F@+1283: GGTCCACCAACATCTTCTTGGAG	*EcoRI* *PstI*	Quantification of hotspots to the right of *YCR061W* (N) Quantification of *YCR061W* main hotspots "N" and also adjacent hotspots to the right

Table S3. Spo11-DSB Mapping libraries used in this study. Mreads refers to million mapped Read 1 ends.

Shorthand Genotype	Library ID	FASTQ ID	Mreads
sae2Δ	MJ315_WT_1_6h	MJ315_S1_L001	*3.29*
sae2Δ	MJ315_WT_2A_6h	MJ315_WT_2A_6h	*8.70*
sae2Δ	MJ315_WT_3_6h	MJ315_WT_3_6h	*4.66*
sae2Δ	MJ315_WT_5_6h	MJ315_WT_5_6h	*3.65*
sae2Δ	MJ315_WT_7B_6h	MJ315-WT_8B_6h	*1.56*
sae2Δ	MJ315_WT_7C_6h	MJ315-WT_8C_6h	*2.12*
sae2Δ tel1Δ	VG402_tel1D_1A_6h	VG402_S6_L001	*4.02*
sae2Δ tel1Δ	VG402_tel1D_1B_6h	VG402_tel1D_1_6h	*5.51*
sae2Δ tel1Δ	VG402_tel1D_2_6h	VG402_2_tel1D_6h	*4.62*
sae2Δ tel1Δ	VG402_tel1D_3_6h	VG402_tel1D_3_6h	*3.84*
sae2Δ tel1Δ	VG402_tel1D_4_6h	VG402_tel1D_4_6h	*4.55*
sae2Δ ndt80Δ	MJ962_ndt80D_1_6h	MJ962_1 - MJ962-1_S4_L001	*6.07*
sae2Δ ndt80Δ	MJ962_ndt80D_2_6h	MJ962_2 - MJ962_ndt80D_2_6h	*5.31*
sae2Δ ndt80Δ	ccLLR9_MJ962_sae2Dndt80D_TC10_6h	ccLLR9_MJ962_sae2Dndt80D_TC10_6h	*4.93*
sae2Δ ndt80Δ	ccLLR17_MJ962_sae2Dndt80D_TC17_6h	ccLLR17__MJ962_sae2Dndt80D_TC17_6h	*4.55*
sae2Δ ndt80Δ tel1Δ	MJ965_ndt80Dtel1D_1_6h	MJ965_1 - MJ965-1_S5_L001	*5.54*
sae2Δ ndt80Δ tel1Δ	MJ965_ndt80Dtel1D_2_6h	MJ965_2 - MJ965_ndt80Dtel1D_2_6h	*4.68*
sae2Δ ndt80Δ tel1Δ	ccLLR2_MJ965_sae2Dndt80Dtel1D_TC5_6h	ccLLR2_MJ965_sae2Dndt80Dtel1D_TC5_6h	*4.90*
sae2Δ ndt80Δ tel1Δ	ccLLR10_MJ965_sae2Dndt80Dtel1D_TC10_6h	ccLLR10_MJ965_sae2Dndt80Dtel1D_TC10_6h	*5.48*
sae2Δ ndt80Δ tel1Δ	ccLLR18_MJ965_sae2Dndt80Dtel1D_TC17_6h	ccLLR18_MJ965_sae2Dndt80Dtel1D_TC17_6h	*3.65*
sae2Δ ndt80Δ spo11-Y135F	Spo11-yf-BL13-GB21-6hr	BL13_GB21_6hr	*10.86*

Table S4. Hotspot calling statistics in various averaged libraries

TEMPLATE	STRAIN BACKGROUND	SIGNAL CUTTOFF	NUMBER OF CALLED HOTSPOTS	NUMBER OF HOTSPOTS AFTER rDNA HOTSPOT REMOVAL	NUMBER OF SHARED HOTSPOTS WITH NEALE TEMPLATE
PAN (2011)	SK1 background WT HA-tagged Spo11	0.193 HpM/bp	3601	NA	3195
MOHIBULLAH (ref)	SK1 background WT ProtA-tagged Spo11	> 0.2 RPM per bp	3910	NA	3323
NEALE	*sae2Δ ndt80Δ* & *sae2Δ ndt80Δ tel1Δ*	0.193 HpM/bp	3486	3473	–
NEALE SPO11-YF	*sae2Δ spo11-Y135F*	0.125 HpM/bp	110	109	32

**Hotspot general parameters: Hann smooth width = 201 bp ; Hotspot merging < 200 bp ; Min mapped reads = 25 ; Min length = 25 bp*